Lawrence Berkeley National Laboratory

Recent Work

Title

DEVELOPMENT OF A SUPERSONIC 0(3PJ), 0(1D2) ATOMIC OXYGEN NOZZLE BEAM SOURCE

Permalink

https://escholarship.org/uc/item/8zb0m4xs

Author

Sibener, S.J.

Publication Date

1979-09-01

Lawrence Berkeley Laboratory
UNIVERSITY OF CALIFORNIA

Materials & Molecular Research Division

DEVELOPMENT OF A SUPERSONIC O(^{3}P$_J$), O(^{1}D$_2$) ATOMIC OXYGEN NOZZLE BEAM SOURCE

Steven J. Sibener, Richard J. Buss and Yuan T. Lee

September 1979

DISCLAIMER

DEVELOPMENT OF A SUPERSONIC $O(^3P_J)$, $O(^1D_2)$ ATOMIC OXYGEN NOZZLE BEAM SOURCE

Steven J. Sibener[*], Richard J. Buss and Yuan T. Lee

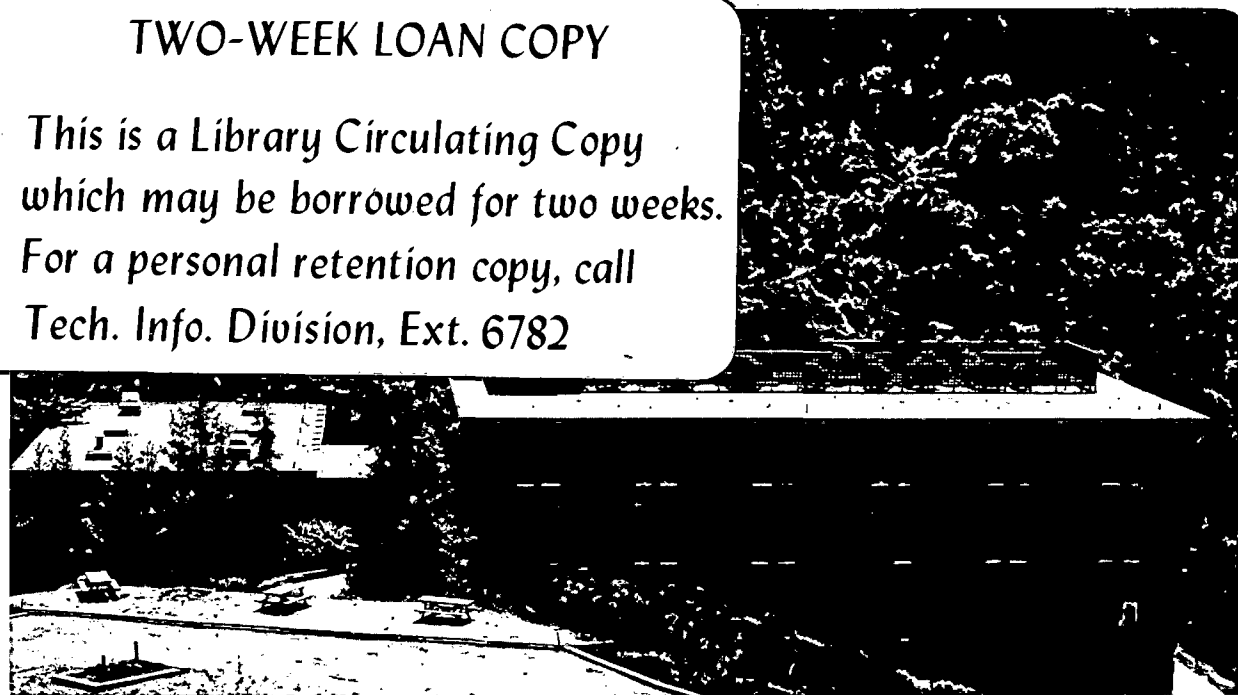Materials and Molecular Research Division
Lawrence Berkeley Laboratory

and

Department of Chemistry
University of California
Berkeley, California 94720

ABSTRACT

A high pressure, radio frequency discharge nozzle beam source has been developed for the production of very intense ($\geq 10^{18}$ atoms sr^{-1} sec^{-1}) supersonic beams of oxygen atoms. An efficient impedance matching scheme has been devised for coupling the radio frequency power to oxygen-rare gas mixtures as a function of gas pressure, temperature, and composition. Techniques for localizing the discharge directly behind the orifice of a specially designed quartz nozzle have also been developed. The above combine to yield a beam source which reliably produces a high degree of molecular dissociation in oxygen-rare gas mixtures at pressures up to 350 torr. Atomic

[*] Present address: Bell Laboratories, 600 Mountain Avenue, Murray Hill, New Jersey 07974

oxygen mean translational energies from 0.14 - 0.50 eV have been achieved using the seeded beams technique with Mach numbers up to 10 being realized. When helium is used as the carrier gas both $O(^3P_J)$ and $O(^1D_2)$ atoms are present in the beam, while only ground state atoms appear to be present in argon seeded mixtures. This paper describes the design, construction, and operation of this beam source and provides a characterization of the atomic oxygen beams it has reproducibly generated in our laboratory.

INTRODUCTION

The interactions and reactions of oxygen atoms are of considerable interest and importance due to the fundamental role they play in combustion processes and atmospheric chemistry. The reactions of ground state $O(^3P_J)$ atoms are of particular interest to researchers studying high temperature combustion processes,[1] laser systems based on the reactions of oxygen atoms which lead to products having vibrationally inverted population distributions,[2] and surface chemistry.[3] A thorough understanding of ground state oxygen atom chemistry is also of immediate practical importance since the space shuttle will orbit the earth at altitudes where the major constituent of the atmosphere is $O(^3P_J)$ atomic oxygen. The reactions of excited state $O(^1D_2)$ atoms are of primary importance due to their major role in the chemistry of the stratosphere.[4] The ability of singlet oxygen atoms to insert in a variety of chemical bonds also makes their chemistry a fascinating subject to explore.[5]

In our laboratory a high pressure, supersonic, radio frequency discharge nozzle beam source has been developed in order to determine the products, energetics, and reaction

dynamics of atomic oxygen reactions in crossed molecular beam scattering experiments. The motivation for constructing this nozzle beam source, rather than relying on much more simple effusive sources, is that supersonic nozzle sources characteristically produce beams of far greater intensity and smaller translational velocity dispersion than effusive sources.[6] The translational energy of nozzle beams can also be varied over a very wide range, from hypothermal to hyperthermal, by using the seeded beam technique.[7] In this technique the peak velocity of the "seed" gas velocity distribution can ideally approach that of the pure "carrier" gas for very dilute gas mixtures. This is accomplished by accelerating or decelerating the seed gas during hydrodynamic expansion through the nozzle by diluting it in either a lighter or heavier carrier gas. Supersonic beams therefore offer several clear advantages over simple effusive sources for conducting dynamical studies in molecular beam experiments.

The successful operation of a discharge beam source depends strongly on the characteristics of its plasma. In particular, the production of a stable and efficiently coupled high pressure discharge for the generation of atomic species is much more difficult than the production of a low pressure (~1 torr) discharge. Impedance matching

of the plasma to the radio frequency power source as a
function of gas pressure, temperature, and composition is
required. Plasma localization directly behind the orifice
must also be achieved in order to limit atomic recombina-
tion before the expansion. Sufficient cooling of the
nozzle in order to prevent melting of its orifice, and
to limit atomic recombination at the nozzle walls (while
not interfering with power coupling to the plasma) is
mandatory. Finally, the high pressure plasma must operate
in a stable, reproducible, and uniform discharge mode
(no beads or streamers) whose temperature is sufficiently
high to generate atomic species, but not high enough to
melt the orifice of the nozzle. The beam source described
in this paper meets all of the above criteria. A boron
nitride skimmer is used and is found to be completely
stable with respect to the seeded atomic oxygen beam.

Other high pressure atomic oxygen beam sources have
been previously reported in the literature. Miller and
Patch[8] have described in detail a radio frequency dis-
charge beam source which produces ~35% dissociation at
60 torr for a 5% oxygen-helium mixture. Gorry et al.[9]
have reported a microwave discharge source with dissocia-
tion characteristics similar to those of Miller and Patch.
The impedance matching scheme, nozzle construction and,

in particular, plasma localization techniques described
in this paper permit a higher degree of molecular dissocia-
tion to be achieved at significantly higher operating
pressures than the sources mentioned above. The current
limitation on the atomic oxygen beam intensity produced
by our source is not atomic recombination at high pressures
but rather the speed of the diffusion pump which backs the
source region. In some cases the characteristics (for
example, gas temperature) of the high pressure plasmas
we have generated to date also become a concern when
pressures exceeding ~400 torr are used. The source has
been operated at pressures exceeding 200 torr for oxygen
helium mixtures with greater than 50% molecular dissocia-
tion, producing atomic oxygen intensities of $\geq 5 \times 10^{18}$ atoms
$sr^{-1} sec^{-1}$. Oxygen-argon mixtures have been discharged at
pressures exceeding 300 torr with greater than 80% dissocia-
tion, and with measured atomic oxygen intensities of ca.
5×10^{17} atoms $sr^{-1} sec^{-1}$.

The beam source described in this paper was originally
designed in order to produce intense supersonic beams of
ground state $O(^3P_J)$ atoms. However, we find that when
dilute oxygen-helium mixtures are discharged the beam is
composed of a mixture of atomic quantum states including
excited state $O(^1D_2)$ atoms. The concentration of $O(^1D_2)$
atoms in this beam has proven to be of sufficient magnitude

to permit the study of $O(^1D_2)$ reactions in crossed molecular beam experiments. This exciting development will eliminate the need to use powerful and expensive UV pulsed lasers for the photodissociative production of $O(^1D_2)$ atomic beams when the presence of other chemical species in the beam, such as $O(^3P_J)$ and $O_2(^1\Delta_g)$, will not seriously complicate the chemistry under study.

SOURCE DESIGN AND CONSTRUCTION

A cross-sectional view of the source mounted in the differential pumping region of our universal scattering machine is shown in Fig. 1, with an enlarged view of the internal source components and nozzle tip appearing in Fig. 2. The important design and construction consider- ations which led to this final form of our plasma beam source will now be discussed.

A. Nozzle Construction

The first question to be dealt with was that of nozzle material. Quartz and alumina were the two materials con- sidered based upon their relatively high melting points. Initially 99.8% purity alumina tubes[10] with laser drilled holes were tested. They were unsatisfactory for two reasons.

They tended to crack when subjected to large thermal gradients, and arcing occurred between the outer surface of the alumina tubes and the radio frequency coupling coil whenever the outer diameter of the tube came into physical contact with the coil. After this brief test period it was decided that quartz nozzles would have to be fabricated. The final shape of these nozzles can be seen in Fig. 1(c) and Fig. 2(c). A water cooling jacket was incorporated in our final nozzle design to prevent the quartz orifice from melting and enlarging during the expansion of the extremely hot gas mixture. The nozzle tip geometry shown in Fig. 2(L) was ultimately found to be stable with respect to orifice enlargement. Here the water coolant flows directly over the junction between the inner, plasma containing tube (6 mm O.D. commerical grade fused quartz, 1 mm wall thickness, as bubble free as possible) and the quartz water jacket (12 mm O.D., 1 mm thick). The short tip on the front of the inner tube is approximately 1 mm long and allows the coolant to flow as close as possible to the orifice. This is important due to the poor thermal conductivity of quartz. In addition to preventing melting of the nozzle, water cooling is also desirable since the efficiency of

quartz to promote atomic oxygen recombination decreases with lower surface temperatures.[11]

Low electrical conductivity water of 5 µmho/cm conductivity is used as the nozzle coolant and is flowed through the concentric water jacket at a rate of 10 cm^3/sec. Use of regular conductivity water as the coolant is precluded due to excessive radio frequency power loss to the water. As an added benefit, the cooling jacket completely eliminated the arcing problem mentioned above. This arcing was found to occur for both alumina and quartz plasma containing tubes which were not physically separated from the coil by another insulating layer.

The nozzle fabrication procedure is quite reproducible and is briefly outlined here. The graded seal water inlet and outlet arms along with their solid quartz support rod (Fig. 2, E,G,H,I) are initially assembled and put aside for later use. Next, the inner tube is prepared. This preparation consists of three operations: Flaring one end just to clear the I.D. of the outer tube, creating the important tip on its front end (Fig. 2, L), and fusing three small quartz physical support standoffs to the inner tube. These three small "droplets" of quartz should be placed at 120° with respect to each other and positioned from 6-7.5 cm from the tip. They should be sized just to clear the

I.D. of the outer tube and will be used to hold the inner tube concentric with the water jacket. The inner tube assembly is then slid inside of the outer tube with the outer tube extending past the inner front tip by about 5 cm. At this time the three inner tube support standoffs are fused to the I.D. of the outer tube and should be adjusted until the two tubes are concentric. A ring seal is then made between the flared rear end of the inner tube and the outer tube. Quartz tubulations are then blown onto the outer tube which will ultimately be attached to the water coolant arms. Next, the 5 cm outer tube extension is pared off with a torch and a carbon tool. The objective of this is to create a 1 mm thick quartz face which seals off the front of the outer tube without touching the tip of the inner tube. This front surface should be as perpendicular as possible to the concentric tube axis and should be just shy of touching the inner tip. The assembly is completed by joining the inner tip and the newly created quartz nozzle face with a ring seal.

At this point the most critical stage of the nozzle fabrication procedure is carried out. The nozzle assembly, with the water arms still detached, is mounted in a glass-blower's lathe. The orifice is now blown on a spinning lathe in an operation requiring two people. Using a

hydrogen-oxygen flame the front face of the nozzle is
heated at a wide angle until the quartz is ready to be
blown. The flame is then quickly removed and a hole is
blown in the tube. This hole should be slightly larger
than the desired diameter of the nozzle orifice. One
person now locally heats the tip of the quartz nozzle
while the other simultaneously views the hole diameter
with a 60X power measuring microscope. The hole is allowed
to shrink slowly until the desired diameter is reached.
Hole size readjustment can be carried out with this pro-
cedure until the orifice is within 0.005 mm of the desired
diameter.

When an orifice of the desired size is obtained its
straightness is always checked by placing a small positive
pressure of oxygen behind the nozzle. This produces a
small oxygen jet at the orifice. The shape profile of this
jet is then made visible by aiming a small gas torch at the
jet while the entire nozzle is rotated in the lathe. If
any wobble or precession of the flame jet is detected
the orifice is reblown. We consistently find that the
straightest orifices are produced by shrinking a larger
diameter hole down to the proper size rather than by
enlarging a hole which is too small. Nozzle diameters
are typically 0.076 mm for ogyxen-argon discharges and

0.191 mm when oxygen-helium mixtures are used. The reasons
for using two differently sized nozzles will be covered in
the next section of this paper. Nozzle assembly is then
completed by attaching the coolant inlet and outlet arms
to the water jacket and by briefly etching the inner quartz
tube with a dilute solution of hydrofluoric acid. This
acid rinse is believed to inhibit atomic recombination on
the walls of the tube.[12]

B.   Electrical Design

Two distinct radio frequency circuit arrangements can
be used for generating electrodeless discharges in gases.[13]
One arrangement involves the use of a self-excited power
oscillator. In this configuration the tube containing
the gas to be discharged is placed through the tank coil
of a free running power oscillator. Large amounts of radio
frequency power can be coupled to a discharge in this manner,
but it is inherently inefficient and can pull out of
oscillation as the circuit loading changes. Loading varia-
tions can occur when the pressure of the discharge is
varied over several hundred torr. Its most serious draw-
back is that impedance matching between the plasma and the
oscillator's circuitry, while the oscillator is in opera-
tion, is very difficult to achieve. The other circuit

option, and the one which we have adopted, uses a driven oscillator-amplifier arrangement in which a variable frequency oscillator is separated from the load by one or more stages of amplification. In this manner the oscillator is very well isolated from load variations induced by changing plasma characteristics. More importantly, this arrangement allows the impedance of the gaseous discharge to be carefully matched to that of the radio frequency electronics. This ensures efficient use of the available radio frequency power. It also offers the desirable option of separating the electronics from the plasma coupling LC tank circuit.

The radio frequency (hereafter, RF) power for our beam source is supplied by a Viking Valiant radio transmitter which can deliver a maximum output of 140 watts over a continuously variable frequency range several hundred kilohertz wide, centered at 14 MHz. (It is difficult to obtain wide fequency tunability in the coupling tank circuit of this beam source at frequencies significantly higher than 25 MHz due to the stray capacitance associated with its physical layout.) When higher power levels are required a linear amplifier capable of providing RF output levels of up to ca. 750 watts is used. However, RF levels exceeding 200 watts are rarely needed due to the highly

efficient impedance matching scheme which is employed.
The plasma coupling tank coil and capacitor can be seen
in Fig. 1. The variable air capacitor (Bud #1615, 0-75
pf, 0.762 cm airgap) is mounted outside of the vacuum to
facilitate the initial frequency matching of the coupling
tank circuit to the electronics. A grid dip meter is
used for this preliminary tuning of the beam source.

A novel impedance matching scheme is used which
enables the source to operate routinely at a standing
wave ratio (SWR) of less than 1.05:1. Impedance matching
is necessary since the effective plasma impedance which
varies as a function of plasma condition, is much larger
than the 50 ohm output impedance of the electronics.
Figure 3 shows a schematic outline of the impedance
matching circuitry which can best be understood when
viewed in two stages. First, a variable group tap on
the tank coil (Fig. 2,A) is used to produce a large
stepdown of the plasma impedance, as seen by the RF
electronics, ideally to 50 ohms. This large stepdown
of the plasma impedance is accomplished with the coupling
coil-ground tap arrangement acting as an RF autotransformer.
Since this is an RF circuit, the impedance transformation
(for a uniformly wound coil) goes only approximately[14] as
the square of the turns ratio, $(N/n)^2$, where N is the total

number of coil turns and n is the numbers of turns from
the rear of the coil to the ground tap. This impedance
transformation creates a large voltage stepup at the
front of the coil (nearest the nozzle tip) and necessi-
tates the use of a high voltage ceramic feedthrough for
the RF return, as is shown in Fig. 1,J. This large,
but approximate impedance transformation allows the RF
power to be delivered to the beam source from a remote
location by RG-213/U coaxial cable. In a procedure which
must be carried out only once when the source is first
constructed, the source must be repeatedly tested with
the position of the ground tap varied in order to deter-
mine optimum placement of the ground tap. This placement
is found by noting the tap location which minimizes the
standing wave ratio between the final RF amplification
stage and the tank circuit. For the source geometry shown
in Fig. 1 the optimum tap locations are 2-1/4 turns from
the rear end of the coil for discharging oxygen-helium
mixtures at 200 torr, and 2-1/2 turns from the rear end
for oxygen-argon discharges operated at up to 350 torr
total pressure. Standing wave ratios are always less than
3:1 with these tap locations and are frequently much
lower.

Next, a PI-network, series capacitor arrangement is used to critcially fine tune the impedance match until standing wave ratios of 1.1:1 or less are achieved. This circuit arrangement represents a quite diverse impedance matching scheme in that the PI-network can be used to match purely resistive load mismatches while the series capacitor can be used for tuning out any reactive impedance components presented to the RF electronics by the plasma coupling tank circuit. We find that the circuit impedance changes when the plasma is first started, varies rapidly as the nozzle pressure is raised from 1 to about 50 torr, and then varies more slowly as the pressure is further raised to several hundred torr. It is also found to vary with RF power level and gas composition. These impedance variations arise from the changing reactance of the coupling coil, which can be attributed to the changing permeability of the region inside the tank coil. In the original design and testing of this circuit a highly variable PI-network, series capacitor arrangement was constructed having an intended circuit Q of 10. The equations used for the design of the PI-network[15,16] were (for $R_1 > R_2$):

$$X_{C1} = \frac{R_1}{Q} \tag{1}$$

$$X_{C2} = R_2 \sqrt{\frac{R_1/R_2}{Q^2+1 - (R_1/R_2)}} \qquad (2)$$

$$X_{L1} = \frac{QR_1 + (R_1 R_2/X_{C2})}{Q^2 + 1} \qquad (3)$$

where X_{C1}, X_{C2}, and X_{L1} represent the reactances of the components shown in Fig. 3, R_1 and R_2 represent the impedances of the tank circuit and RF electronics, respectively, and Q is the quality factor of the matching network. Particular attention should be focused on R_1 in the above equations, noting that it is related to the stepped-down resistive impedance of the gaseous discharge. The series capacitor, C3 in Fig. 3, completes the impedance matching circuitry and is varied during the SWR minimization procedure in order to eliminate any reactive components of the tank circuit impedance. In the initial design of this circuit both C1 and C2 were variable up to 750 pf and were comprised of several high voltage ceramic and air variable capacitors which were connected in parallel. Also in the initial design, capacitor C3 was variable up to 250 pf while the inductor, L1, had a maximum calculated inductance of 6.9 µH. It consisted of a 7.6 cm diameter by 15.2 cm long, 15 turn tapped coil which was constructed out of 0.64 cm diameter copper tubing. The tap could be attached to

the coil in 30 positions distributed evenly along the length of the coil, making L1 values well below 1 μH possible. This circuit worked very well but was eventually replaced (for ease of operation) by a slightly modified, commerically available network.[17] In this commerical unit C1 and C3 are 20-245 pf air variable capacitors, C2 is variable in discrete jumps up to 2160 pf, and L1 consists of a 5.1 cm diameter by 9.1 cm long, 9 turn coil which is tapped on its fifth turn for 14 MHz operation. The tuning of these impedance matching circuits is greatly facilitated by the continuous use of in-line RF watt-meters and a standing wave ratio bridge. Power coupling to the plasma is found to be extremely efficient (> 99%) and power levels must be carefully limited in order to avoid melting the orifice of the quartz nozzle. Stray RF fields radiating from the source have been minimized by completely enclosing the top of the beam source with electrically grounded copper mesh.

Figure 4 shows a block diagram of the RF circuitry. Note that the beam source is always operated in a doubly interlocked condition. Nozzle meltdown protection is provided by a paddlewheel flow switch[18] which can quickly turn off the RF power should the nozzle coolant flow rate drop below a predetermined level. Similarly, the RF

electronics are protected by a fast electronic meter relay
which has been incorporated into an SWR bridge circuit.
This relay can rapidly turn off the RF power when the SWR
rises above some preset value, which is usually chosen
as an SWR of 2.5:1.

Finally, we have been successful in localizing the
plasma directly behind the orifice of the nozzle. This
spatial localization of the plasma is of critical importance
if an atomic beam of high molecular dissociation is to be
produced from a high pressure discharge. Without this
plasma localization at the nozzle tip extensive atomic
recombination would occur. The localization has been
achieved by placing around the nozzle tip (outside of the
water jacket and *not* along the front face of the nozzle)
a carefully shaped, electrically grounded block of aluminum
(Fig. 2,J). The discharge appears to change gradually
from an inductively coupled plasma at low pressures to a
capacitively coupled discharge at high pressures. This
coupling at high pressures occurs beween the front, small
diameter tank coil turns, and the grounded aluminum block.
As this coupling becomes stronger the plasma localizes
towards the front of the discharge tube. Photographic
studies have shown that the discharge region protrudes
past the front plane of the grounding block and actually

extends up to the nozzle tip, ensuring a high degree of molecular dissociation directly behind the nozzle at high pressures.

The tank coil (Fig. 2,D) has been differentially wound in order to further localize the plasma and to increase its energy density at high pressures. The first 6-1/2 coil turns nearest to the nozzle tip are 1.37 cm I.D. by ~6.0 cm long while the 5 large turns are 5.08 cm I.D. by ~6.5 cm long. The larger turns decouple from the plasma as the pressure is raised, and therefore the energy density of the localized plasma is considerably increased. The coil is constructed of 0.32 cm O.D. copper tubing and was wound around correctly sized metal tubes on a low-speed lathe. The small diameter coil windings should be uniformly spaced and carefully shaped in order to avoid any inhomogeneities in the RF field. These inhomogeneities, if present, can cause the uniform plasma to collapse into streamers at high pressures. The coil is water cooled with low electrical conductivity water at a flow rate of 4 cm^3/sec in order to improve the long term mechanical, and hence electrical, stability of the tank circuit. Also note that the entire tank circuit, as seen in Fig. 1, is floated with respect to electrical ground. That is required if the RF coupling and localization schemes, as described here, are to be effectively used.

The pumping requirements for this beam source vary greatly depending upon the gas mixture which is to be used. It was originally pumped by a 4200 l/sec diffusion pump which was separated from the source by a sliding gate valve. This pumping arrangement was recently replaced by an 8000 l/sec pump which was directly joined to the source. This large pumping speed is desirable while running high pressure oxygen-argon mixtures, for which the pressure must be kept below 7×10^{-5} torr. For higher background pressures the RF power decouples from the nozzle and a glow discharge of the entire source region occurs. This glow discharge is a problem which currently constrains the nozzle orifice diameter to 0.075 mm for gas mixtures containing argon. Nozzle pressures exceeding 350 torr have been successfully run with argon as the carrier gas. Helium seeded beams do not have this operational constraint. This allows much larger orifices to be used for helium seeded beams operating at high nozzle stagnation pressures, provided that sufficient pumping speed is available for backing the foreline of the diffusion pump.

Significant effort was also devoted to fabricating a skimmer which would not degrade when exposed to the atomic oxygen beam. Skimmers made of electrically conducting

materials, including stainless steel, were not stable over long time periods due to sputtering by high energy ions. Apparently, ions emanating from the nozzle were being accelerated towards the ground potential of these metallic skimmers. Boron nitride[19] skimmers with 0.81 mm openings were found to be completely stable with respect to the oxygen beam. The electrical insulating properties, machinability, and density of boron nitride actually make it an ideal skimmer material for use with this beam source.

C. Source Operation

The tuning and operating of the beam source is quite straightforward. The plasma coupling tank circuit should first be tuned to the desired resonant frequency by adjusting the tank circuit's variable air capacitor, which is mounted on top of the beam source. The resonant frequency of this circuit can be easily monitored by placing the probe of a grid dip meter adjacent to the tank circuit capacitor, which is conveniently located outside of the vacuum. During this tune-up procedure the coaxial cable which brings the RF power to the source should be disconnected from the source to ensure correct tuning of the circuit. Next, the RF power should be turned on (~100 watts) with the impedance matching network and high power amplifier temporarily bypassed, and with the

nozzle evacuated to $\leq$ 1 torr. The variable frequency
oscillator is then varied until the SWR between the beam
source and the electronics is minimized. If the discharge
is not ignited when the SWR minimum is reached the RF
power should be quickly switched off and then on again.
Invariably the discharge will be ignited by this procedure.
Gas should now be flowed into the nozzle while simultane-
ously retuning the oscillator's frequency to maintain the
SWR at a minimum. When pressures on the order of 100 torr
are reached, the RF power level may be safely increased to
sustain the discharge at higher pressures. The pressure
may then be further increased, again with the simultaneous
retuning of the RF electronics, until the final operating
pressure is reached. We consistently find that the
resonant frequency of the plasma coupling circuit increases
slowly with increasing gas pressure. As an example of
this, a 5% O_2-He, 130 watt discharge is found to require a
0.006 MHz frequency increase when its pressure is raised
from 120 to 220 torr. At this point the plasma should be
switched off, the gas mixture in the beam source evacuated,
and then the impedance matching circuitry along with any
high power amplifiers inserted in-line. The source can
now be reignited and tuned for optimum performance
at high RF power levels. After a few minutes of
operation at the final power and pressure settings the

electronics should again be slightly retuned to correct
for any drift during this initial stabilization period.
It should be clearly stated here that the minimum SWR
which can be achieved *before* the matching network is
connected is completely dependent on the placement of
the coupling coil's ground tap (Fig. 2,A). As was dis-
cussed earlier, the correct location for this tap must be
found in a trial and error process which need be done only
once when the source is initially constructed.

After the overall tuning procedure has been com-
pleted the source can be operated without further major
retuning for a period lasting several weeks. Typically
the source is turned on by evacuating the nozzle to about
1 torr, switching on the RF power, and rapidly increasing
the pressure to the desired operating level. Within a few
minutes of reigniting the discharge the operating
characteristics always return to their steady state value.
Most importantly, the beam characteristics are extremely
reproducible for day to day operation of the source,
allowing experimental scattering data to be taken over a
period several weeks long if necessary, without concern
for fluctuating beam characteristics. The quartz orifice
does not enlarge at all when the source is operated at
the power levels discussed in the next section of this

paper. However, sputtering of the front surface of the
quartz nozzle does place a lmit on the lifetime of any
given nozzle. This sputtering results when ions which
leave the nozzle are accelerated back towards its front
surface by the large RF fields present in that region.
Periodic visual inspections of the nozzle tip are carried
out to monitor the nozzle degradation. The nozzles are
replaced when the sputtering errosion becomes severe.
They can be recycled by rebuilding the nozzle face and
reblowing the orifice. Some of the ions which emanate
from the nozzle actually pass through the skimmer. These
are deflected out of the beam by a 5000 V/cm deflecting
field which is placed before the collision region of
our apparatus (Fig. 1,N). The beam characteristics for
different nozzles operated under the same conditions
have been found to be fairly reproducible, with slight
differences in Mach number and peak velocity being noted.
These differences can be attributed to the slight coil
shape and positioning changes which invariably occur
during each reassembly of the beam source.

BEAM CHARACTERIZATION

    A.   Confirmation of Atomic Oxygen Production

    The atomic oxygen beams produced by this beam source have been thoroughly characterized in order to improve our understanding of the source's operation and to optimize its performance. A wide variety of diagnostic techniques have been used for this analysis. Chronologically, our first goal was to experimentally verify the presence of oxygen atoms in the terminal beam. This was unambiguously demonstrated by measuring the differential elastic scattering cross section for O-He and O_2-He in our universal crossed molecular beam apparatus.[20] In these measurements the elastically scattered mass 16 and mass 32 number densities were recorded, with the discharge on, when the oxygen beam was crossed at 90° with a supersonic beam of pure helium. For this preliminary experiment a 5% O_2-Ar mixture was discharged in the source at 95 torr total pressure by 95 watts of RF power. The Newton velocity diagrams[21] for these two collision systems are shown in Fig. 5a, and clearly reveal how the presence of atomic oxygen in the terminal beam can be confirmed by these experiments. They show that the heavier molecular oxygen is kinematically constrained to scatter within a LAB angle

of approximately 24° while the lighter atomic oxygen, if present in the beam, could be scattered to 44° in the LAB reference frame. These differential cross sections would also be expected to have a rather broad peak in the vicinity of these cutoff angles due to the nature of the transformation Jacobian which relates the LAB and Center-of-Mass reference frames. Figure 5b shows the experimentally measured differential elastic cross sections for these two systems. The mass 16 (O-He) scan can be seen in this figure to have a qualitatively different shape from the mass 32 (O_2-He) scan. This difference indicates that the mass 16 signal does not exclusively come from the dissociative ionization of elastically scattered molecular oxygen in the ionizer of our quadrupole mass spectrometer. More importantly, the mass 16 scan does in fact peak and begin to fall off around 40° while for the mass 32 scan this occurs at 20°, in excellent agreement with the shapes predicted from the most probable Newton diagrams shown in Fig. 5a. The experimental curves actually extend past the predicted cutoff angles due to the finite spread of velocities in the two beams. The O-He experimental curve shown in Fig. 5b has been corrected for the dissociative ionization of elastically scattered molecular oxygen. We

conclude from the above data that oxygen atoms are definitely present and, in fact, they are more abundant than oxygen molecules in the terminal beam produced by our high pressure, RF discharge beam source.

B. Molecular Dissociation

The extent of O_2 dissociation in the terminal beam has been carefully measured for several oxygen-rare gas mixtures as a function of gas pressure and RF power. These measurements were made in our crossed beam apparatus with the triply differentially pumped mass spectrometer looking directly along the beam axis. The relative O and O_2 number densities were actually measured by integrating the time-of-flight spectra of masses 16 and 32. We have opted to integrate these time-of-flight spectra rather than use our usual particle counting electronics in order to eliminate any possible contributions from VUV photons and high energy ions in the detected signals. This separation of the true signal from VUV photon and high energy ion contributions can easily be made in the time regime with our time-of-flight (herafter, TOF) instrumentation since the interferring factors always have much shorter flight times that the true signal. The ion deflecting field mentioned earlier was held at a field strength of 5000 V/cm during these measurements and was

found to deflect virtually all of the ions emanating from the beam source. Only during very high power operation of the beam source did a few high energy ions apparently reach the detector.
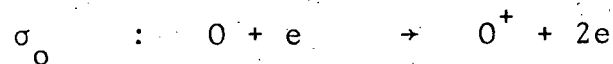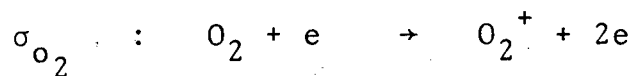
The TOF apparatus used in these studies consisted of a 17.78 cm diameter aluminum disk having four equally spaced 0.5 mm or 1.0 mm slots around its circumference. The disk was rotated at either 300 or 350 Hz during data acquisition. The detector aperature was narrowed to 0.125 mm diameter, and the distance between the TOF disk and the electron bombardment ionizer was 18.4 cm. The ionizer and quadrupole mass spectrometer have been previously described in detail,[20] and the ionizer's emission current was set sufficiently low to eliminate any space charge perturbations of the detected signal intensities and velocity distributions. A 256-channel scaler interfaced to an on-line NOVA minicomputer was used to record signal intensity as a function of flight time. The scaler was usually set at 2 μs dwell time for the helium mixtures and 4 μs for the argon mixtures.

The extent of molecular dissociation in the terminal beam was calculated with the following two equations:

$$ R = \frac{N_o}{N_{o_2}} = \frac{(\sigma_D/\sigma_{o_2})}{\eta} \left(\frac{\sigma_{o_2}}{\sigma_o} \right) \left(\frac{I_o - \eta I_{o_2}}{I_{o_2}} \right) \qquad (4) $$

$$\text{Percent Dissociaton} \quad = \quad \frac{R}{R+2} \qquad\qquad (5)$$

where I_O and I_{O_2} are the experimentally observed mass 16 and 32 number densities, η is the experimentally observed I_O/I_{O_2} count ratio with the discharge off, and the cross sections represent the following processes:

$$\sigma_{O_2} \quad : \quad O_2 + e \quad \rightarrow \quad O_2^+ + 2e$$

$$\sigma_O \quad : \quad O + e \quad \rightarrow \quad O^+ + 2e$$

$$\sigma_D \quad : \quad O_2 + e \quad \rightarrow \quad O + O^+ + 2e$$

For ionization with 250 eV electrons: σ_{O_2} = 1.52 Å^2, σ_O = 1.15 Å^2, and σ_D = 0.88 Å^2.[22,23] In their paper Miller and Patch[8] have used an equivalent expression for R, and have discussed the approximations and assumptions leading to the use of equations (4) and (5). The $(\sigma_D/\sigma_{O_2})/\eta$ term corrects for any differential detection of masses 16 and 32 by our detector. This difference in detection probability, if present at all, is partially due to the differential transmission of m/e = 16 and 32 through the quadrupole mass filter of our detector.

Figure 6 shows the pressure dependence of O_2 dissociation for four oxygen-rare gas mixtures under a variety of

RF power settings. These curves reveal the unique operating characteristics of this beam source. The molecular dissociation is seen to depend only weakly on the nozzle stagnation pressure, varying only a few percent over a several hundred torr pressure range. The actual extent of molecular dissociation in the beam is also found to be quite high over this large pressure range. Argon seeded mixtures regularly achieve moelcular dissociation levels of 80-90% while helium seeded mixtures operate with 50-65% dissociation. The weak pressure dependence and high dissociation levels described here can undoubtedly be attributed to the spatial localization of the plasma at the tip of the quartz nozzle. The dissociation percentages shown in Fig. 6 have been found to be reproducible to within about 5% for data taken over a several month time period with many different nozzles. Further examination of the curves shown in Fig. 6 indicates that the dissociation versus pressure curves for identical gas mixtures discharged by different RF power levels have similar slopes, with the higher power curves shifted to slightly greater dissociation. The 10% oxygen mixtures also appear to exhibit slightly lower dissociation values than their more dilute counterparts.

Figure 7 shows even more clearly the effect of RF power and O_2 concentration on molecular dissociation.

Increasing the RF power from 130 to 195 watts is seen to raise the dissociation level by at most 10% for three different gas mixtures. The two upper curves of this figure also show that the extent of molecular dissociation is only mildly influenced by raising the O_2 concentration from 5% to 10% when argon is used as the carrier gas. The 10% O_2-Ar mixture is seen from Fig. 7 to exhibit the same RF power dependence as the 5% O_2-Ar mixture, with its dissociation precentage lower by about 10%.

The information related in Figs. 6 and 7 has been very useful for optimizing the performance of our oxygen atom beam source. The very weak pressure dependences shown in Fig. 6 indicate that the nozzle stagnation pressure should be held as high as possible, subject to the limitations of plasma stability and pumping speed availability, without worry of severe recombination. These figures also tell us that 10% O_2-rare gas mixtures should be used rather than more dilute mixtures in order to increase the flux of oxygen atoms leaving the nozzle. Finally, Fig. 7 informs us that power levels approaching 200 watts should be quite adequate for dissociating molecular oxygen in seeded argon and helium gas mixtures. This is fortunate since power levels exceeding 200 watts lead to orifice enlargement when argon is used as the carrier gas. Power levels

exceeding 200 watts also appear to accelerate the quartz sputtering rate at the nozzle face for all gas mixtures tested.

C. Velocity Analysis

The true, undistorted atomic oxygen velocity distributions produced by our beam source have been recovered from the convoluted experimental TOF distributions by correcting the observed spectra for instrumental broadening effects (shutter function and finite ionizer length) and ion flight time offset. The peak velocity and Mach number of these distributions have been found to vary with both nozzle stagnation pressure and RF power level. Figure 8 indicates the dependence of peak velocity on nozzle pressure for seven different gas mixture - RF power combinations. The effect of seeding is immediately apparent here, with the oxygen seeded in helium beams having much higher velocities than the oxygen seeded in argon gas mixtures. The mean energy of the atomic oxygen beams generated in our laboratory span the range from 0.1 - 0.5 eV, with the highest energies being obtained for 5% O_2-He mixtures discharged with 200 watts. The shape of the curves shown in Fig. 8 indicates that velocity "slippage" occurs between the oxygen and carrier gases during the hydrodynamic nozzle expansion. Velocity slippage occurs when

the collision frequency is too low during the nozzle expansion to effect complete momentum and energy equilibrium between the seed and carrier species. Slippage is especially typical of low pressure, high temperature expansions due to the relatively low number density these systems have in the vicinity of the nozzle orifice. When slippage occurs it can usually be minimized by increasing the pressure behind the nozzle, which increases the number of collisions which occur during the expansion. This behavior is clearly seen in Fig. 8. The mixtures having helium as the carrier gas have their atomic oxygen peak velocities steadily *increasing* with increasing pressure until their terminal velocities are reached at pressures approaching 150-200 torr. The mixtures having argon as the carrier gas behave oppositely from this, with their peak oxygen velocities *decreasing* with increasing pressure until their terminal velocities are reached between 250 and 300 torr. The above behavior is expected since helium serves to accelerate atomic oxygen while argon decelerates atomic oxygen during coexpansion from the nozzle.

The influence of RF power on beam velocity has also been studied and is shown in Fig. 9 for four gas mixtures. In all cases the atomic oxygen velocity is found to increase monotonically with increasing RF power. This in turn

indicates that the effective plasma temperature does in fact rise with increasing RF power. The translational energy of the beam can therefore be tuned over a narrow energy range about 0.1 eV wide by simply varying the RF power used to run the discharge. This tunability may apply to an even broader energy range when power levels exceeding 200 watts are used for running oxygen-helium mixtures.

In these experiments the raw TOF data is always recorded as number density versus flight time. However, TOF spectra are more readily interpretable when displayed as flux versus velocity spectra. A typical TOF spectra is shown in Fig. 10 which represents the velocity distribution of a fast atomic oxygen beam. The correct Jacobian transformation, $1/v^2$, was used for converting this and other spectra from time space to velocity space, while the resulting distributions were then multiplied by v to effect the conversion from number density to flux. The oxygen seeded in helium distribution shown in Fig. 10 has a FWHM of 19% with a Mach number of 9.2 as calculated by a parametric fit to the deconvoluted distribution.[24,25] This should be compared to the width of an effusive beam whose velocity distribution is Maxwellian. Numerical solution of the transcendental equation which defines the two half intensity velocities of the distribution $I(v) \propto v^3 \exp(-v^2/\alpha^2)$

shows that the FWHM of a Maxwellian flux distribution is ~95%. The relatively narrow velocity distributions produced by this beam source are one of its most important characteristics, and are in general indicative of beams produced from supersonic nozzle expansions. The slower oxygen seeded in argon beams have typically ~40% FWHM distributions with Mach numbers ranging from 3 to 4. In the future the use of neon rather than argon as the beam carrier gas may enable narrower moderate energy beams to be produced due to the smaller mass mismatch which exists between neon and atomic oxygen relative to that of argon.

The terminal Mach number of a beam is a parameter which is frequently used for characterizing the width of its velocity distribution. It is defined as the ratio of the mass flow speed to the local speed of sound in the beam, v/c, where $c = (\gamma k T_b/m)^{1/2}$, γ is the usual ratio of specific heats at constant pressure to constant volume, and T_b is the temperature of the beam in the reference frame moving with the bulk velocity, v. For seeded gas mixtures which are expanded in the hydrodynamic regime (Knudsen number < 1) collisions with the carrier gas initially accelerate or decelerate the seed gas depending on whether the carrier gas is lighter or heavier than the seed gas, respectively. Subsequent collisions during the expansion

then serve to "cool" the seed gas and to narrow the width of its velocity distribution.[26] The total number of binary collisions which occur during the expansion is proportional to $n_o D$, the product of the particle number density at the orifice with the orifice diameter. Figures 11 and 12 show how the atomic oxygen Mach number varies respectively with nozzle stagnation pressure and RF power for several operating conditions of the beam source. The nearly linear Mach number versus pressure curves shown in Fig. 11 indicate that the cooling process does vary as described above, and is not complete. It is clear from the slope of the curves shown in Fig. 11 that further velocity distribution narrowing should be possible for operation at still higher stagnation pressures. This statement particularly applies to helium containing mixtures, where the addition of a Roots blower to our pumping system will enable the source to operate with higher nozzle pressures (or with a larger nozzle orifice, which would also increase the terminal Mach number of the beam). Figure 12 shows that the beam Mach number decreases as a function of RF power level. This is not surprising since the number density at the orifice decreases as $1/T$, where T is the effective plasma temperature at the orifice. It is nevertheless important to understand the actual *extent* of Mach

number degradation with increasing RF power since future operation of the beam source at higher stagnation pressures may require the use of higher power levels.

D. Plasma Temperature

The temperature of the gas at the nozzle orifice has been determined for a variety of source operating conditions with two different techniques. The first of these techniques depends on the flux change which occurs when the gas temperature at the orifice is varied. The flux emanating from the orifice at constant stagnation pressure depends on the gas temperature in the following way:

$$\Phi(T) \propto n(T) \cdot v(T) \propto 1/\sqrt{T} \qquad (6)$$

where the particle number density, $n(T)$, varies as $1/T$ and the velocity of the particles emanating from the nozzle, $v(T)$, goes as $\sqrt{T}$. An approximate determination of the plasma temperature can therefore be made by measuring the pressure in the source with the discharge turned on and off:

$$\frac{P_1}{P_2} \propto \frac{\Phi_1}{\Phi_2} \propto \sqrt{\frac{T_2}{T_1}} \qquad (7)$$

A Bayard-Alpert ionization gauge was used for making these
pressure measurements, and the gas temperature with the
discharge off was assumed to be 300K. Using equation (7)
the plasma temperature for high pressure oxygen-helium
mixtures is repeatedly found to range from 800-900K for
130 watt discharges, 850-1100K for 165 watts, and from
1150-1300K for 195 watts. Only a slight pressure dependence
is observed, with the temperature tending to decrease
slowly with increasing pressure. Oxygen-argon mixtures
are found to be considerably hotter: 1300-1500K for 130
watts, 1600-1750K for 165 watts, and 1750-2050K for 195
watt discharges at high pressures. The oxygen-argon dis-
charges also have much stronger pressure dependences than
the oxygen-helium discharges, with their temperatures
rising significantly as the stagnation pressure is lowered.
As a specific example of this a 5% O_2-Ar, 130 watt discharge
was found to increase in temperature from 1400K to 1750K
as the pressure was lowered from 250 torr to 100 torr. For
this reason extreme caution should be taken when igniting
(at low pressures) high power argon discharges. Immediately
after igniting high power argon discharges the pressure
should be quickly raised to at least 100 torr in order to
avoid melting of the quartz orifice. The above temperature
measurements are of course only approximate, but are very
useful for day to day plasma characterization. Also note

that the electron temperatures in the plasma are much hotter than the above translational temperatures, with electron temperatures on the order of 10,000K or higher being achieved in the discharge.

More accurate plasma temperature determinations can be made by monitoring the mole fractions and velocity distributions of the three species (O, O_2, and either helium or argon) which are present in the beam. These temperature determinations may be carried out by assuming the overall energy balance.[27,28]

$$(\Sigma X_i C_{P_i}) T_o = \Sigma X_i C_{P_i} T_{bi} + \frac{1}{2} \Sigma X_i m_i v_i^2 \qquad (8)$$

where X_i is the mole fraction, C_{Pi} the heat capacity, v_i the terminal velocity, m_i the mass, and T_{bi} the terminal temperature of each component of the beam, and T_o is the temperature of the gas at the orifice. The assumptions which must be made in order to calculate T_o from equation (8) have been thoroughly reviewed in Reference 8. The mole fractions of each component have been calculated using the molecular dissociation data which was discussed earlier, taken in conjunction with the known composition of the gas mixture under investigation. Figure 13 shows

the RF power dependence of gas temperature, at constant
pressure, for three different gas mixtures. Once again
we see that the argon containing mixtures generate signifi-
cantly hotter plasmas and exhibit stronger power dependences
than the helium containing ones. The data used in con-
structing these curves were intentionally taken at relatively
high operating pressures in order to ensure the validity
of equation (8). The pressure dependence of gas temperature,
at constant RF power, has also been studied for several gas
mixtures under a wide variety of operating conditions.
These studies again indicate that the gas temperature
decreases with increasing pressure. For example, helium
containing gas mixtures typically decreased 200 degrees,
from about 1000K to 800K, for a pressure change from 100 to
200 torr. Argon containing mixtures also exhibit this
temperature decrease with increasing gas pressure. We also
find that the assumptions which enable equation (8) to be
used for calculating gas temperature appear to break down
at low pressures for argon containing mixtures due to the
poor quality of these expansions. This statement especially
applies to high power, low pressure discharges which contain
argon.

In a final attempt to gauge the true gas temperature at the orifice we have also measured the velocity distribution of a pure helium beam which was produced from a 200 torr, 175 watt discharge. Its peak velocity was found to be 2.83×10^5 cm/sec. For an ideal nozzle expansion of a rare gas, where $v = \sqrt{5kT_o/m}$, this velocity corresponds to a gas temperature of 770K. This temperature can be considered to be in fairly good agreement with the temperatures determined above when we take into consideration the difference in gas composition which exists between this discharge and those previously discussed.

In concluding this section on plasma temperature characterization it should be mentioned that we have encountered some plasmas which were not suitable for generating atomic species. In particular, we have been unable to generate "hot" discharges for gas mixtures predominantly composed of helium when small nozzle orifices of ≤ 0.127 mm diameter were tested. These "cool" discharges would typically have temperatures on the order of only 400K for power levels up to 200 watts. These "cool" discharges are fortunately of little practical concern since orifices of ≥ 0.180 mm diameter are always used for running helium containing mixtures. The rate of gas flow out of the orifice is therefore seen to

influence the mode stability of discharges containing
helium, with faster flow rates stabilizing the hotter
mode (~1000K) relative to the cooler mode (~400K). Argon
containing plasmas also have various discharge modes, with
the two most important modes being the desired "hot mode"
(~1750K) and the destructive "streamer" or "pencil" mode
which can occur for operation at pressures in excess of
400-500 torr at high power levels. This latter mode is
extremely hot and can cause rapid enlargement of the
orifice. The inner diameter of the plasma containing
quartz tube can influence the probability of this "hot
mode" to "streamer mode" transition. The inner tube
dimensions given earlier in this paper were chosen as
a compromise between maximizing power coupling to the
discharge and minimizing the probability of streamer
formation at high pressures.

E. Beam Intensity

Absolute beam flux measurements have been carried out
in a differentially pumped beam source test facility in
which a Bayard-Alpert gauge having a 52 mm sidearm extension
was used as the particle detector. For these measurements
the long sidearm of the detector gauge was pointed directly
into the beam and was terminated with a small 1.58 mm
conical aperature. The pressure rise, ΔP, which is registered

by the gauge when the beam is turned on can be used for calculating the absolute intensity of the beam when the distance between the source skimmer and the detector entrance aperature, d, is accurately known. This intensity determination is possible since the pressure rise, ΔP, reflects the new rate equilibrium which is established between molecules entering the detector and those effusing from it. The rate at which molecules enter the detector can therefore be found by calculating the rate at which molecules effuse out of the detector. This effusion rate can be expressed as: $\Phi = \frac{1}{4} n_o v_o A$, where $n_o = \Delta P/RT$, $v_o = \left(\frac{8kT}{\pi m}\right)^{\frac{1}{2}}$, A is the area of the detector entrance aperature, and T is assumed to be 300K. The long sidearm extension was added to the ionization gauge to ensure the validity of this last assumption. The absolute intensity of the beam in terms of solid angle units can be obtained by dividing Φ by $\Delta\Omega$, the solid angle subtended by the detector aperature, where $\Delta\Omega = A/d^2$. Examination of the above relationships reveals that the actual area of the detector aperature does not influence the outcome of the beam intensity determination as it cancels out in the final step of the calculation. The detector-skimmer distance, d, was fixed at 86.54 mm for these studies. Pure argon discharges which were operated at power levels between 165 and 195 watts at stagnation

pressures up to 350 torr were found to have beam fluxes
of 3.6 x 10^{18} atoms sr^{-1} sec^{-1}. The atomic oxygen mole
fraction present in the terminal beam of 10% O_2-Ar
discharges, run under the same power and pressure
settings as above, is known to be 0.15 from molecular
dissociation experiments. By combining the above data
the absolute oxygen atom flux produced by discharging
oxygen-argon mixtures is found to be ca. 5 x 10^{17}
atoms sr^{-1} sec^{-1}. Pure helium discharges which were
run at 200 torr with power levels again between 165
and 195 watts produced beam fluxes of 5.5 x 10^{19} atoms
sr^{-1} sec^{-1}. Combining this figure with the measured
atomic oxygen mole fraction for 10% O_2-He discharges,
X = 0.10, leads to an absolute atomic oxygen flux of ca.
5 x 10^{18} atoms sr^{-1} sec^{-1} for oxygen-helium discharges.
The pure rare gas beam intensities produced by this source,
as described above, are comparable in magnitude to the
intensities which have been reported in the literature
for other nozzle beam sources.[29,30] The ionization gauge
readings which were used for these and subsequent beam
intensity calculations were corrected for the differences
in gauge sensitivity which exist for the various gases
under study. The gauge readings were actually divided
by 1.19, 0.15, and 0.85 in order to find the true pressure

changes due to Ar, He, and O_2, respectively.[31] These represent the correct gauge sensitivity conversion factors as the detector gauge was calibrated for N_2.

The pressure rises due to oxygen-rare gas beams were also measured in order to perform an approximate check on the atomic oxygen flux estimates described above. Predictions for the seeded beam pressure rises were based on the pure rare gas data, and were calculated in the following way: $\Delta P_{mix}(\text{predicted}) = (X_{RG} + X_{O_2}(\frac{0.85}{S}))\Delta P_{RG}$, where X_{RG} and X_{O_2} represent the rare gas and oxygen concentrations of the gas mixture, ΔP_{RG} is the pressure rise registered by the gauge for a pure rare gas beam run under the same stagnation pressure and RF power settings, ΔP_{mix} is the predicted gauge pressure rise due to the seeded beam, and S is the gauge sensitivity conversion factor for either helium or argon. The measured gauge pressure increases for oxygen-argon discharges agreed well with the predicted gauge deflections, falling consistently within 10% of ΔP_{mix}. However, the measured pressure rises for oxygen-helium beams were usually 20% higher than the predicted gauge deflection. This discrepancy can be explained if the mole fraction of oxygen (O and O_2) along the beam axis is larger in the terminal beam than in the initial gas mixture. This explanation is supported by the fact

that the heavier particles of a seeded gas mixture are preferentially focused on the beam centerline during hydrodynamic nozzle expansion,[32] and are attenuated less than lighter particles in the region between the nozzle orifice and the skimmer. In summary, we therefore find the atomic oxygen flux to be about 5×10^{17} atoms sr^{-1} sec^{-1} for oxygen seeded in argon beams and $\geq 5 \times 10^{18}$ atoms sr^{-1} sec^{-1} for oxygen seeded in helium beams. For these determinations a 40° inner-60° outer cone angle, 0.82 mm diameter boron nitride skimmer was fixed at a nozzle-skimmer distance of 5.08 mm, a second collimating skimmer of 1.04 mm diameter was placed 31.78 mm from the orifice, and a flat slot of variable dimensions was placed 52.76 mm from the orifice in the wall which separated the differential and detector sections of the apparatus. The total gas flow emanating from the nozzle is typically 0.75 torr-1/sec for 200 torr, 165-195 watt oxygen-helium dis-charges (0.191 mm diameter orifice) and 0.25 torr-1/sec for 350 torr, 165-195 watt oxygen-argon discharges (0.076 mm diameter orifice).

The ability of this beam source to produce intense atomic oxygen beams at high pressures, without suffering significant intensity loss due to atomic recombination, is one of its most novel and important operating

characteristics. This behavior is clearly demonstrated
in Fig. 14 where the atomic oxygen number density, as
measured with a quadrupole mass spectrometer, is plotted
as a function of increasing stagnation pressure for four
gas mixture-RF power level combinations. In Fig. 14a
the relative $m/e = 16$ number density is seen to rise
linearly with increasing stagnation pressure over the
entire pressure regimes which were explored for two argon
containing gas mixtures: up to 300 torr for a 5% O_2-Ar,
165 watt discharge and 350 torr for a 10% O_2-Ar, 195 watt
discharge. The 10% O_2-He, 165 watt number density curve
shown in Fig. 14b behaves in a similar manner, up to a
maximum pressure of 200 torr, as those described above.
However, the 5% O_2-He, 130 watt curve shown in this figure
turns over at pressures higher than 200 torr. This indi-
cates that power levels $\geq$ 165 watts should always be used
for running oxygen-helium discharges above 200 torr total
pressure. The $m/e = 16$ curves shown in Fig. 14 have all
been corrected for the slight contributions arising from
dissociative ionization of the molecular oxygen which is
present in the beam. The high pressure segments of these
curves are also representative of the relative atomic
oxygen *fluxes* produced by this source, as a function of
increasing pressure, due to the weak dependence beam velocity
has on gas pressure at high stagnation pressure.

F. $O(^1D_2)$ Production

When dilute oxygen-helium gas mixtures are discharged in this beam source a mixture of atomic oxygen quantum states including ground state $O(^3P_J)$ and excited state $O(^1D_2)$ atoms is present in the terminal beam. When helium is used as the carrier gas the $O(^1D_2)$ flux has in fact proven to be of sufficient magnitude to permit differential reactive scattering experiments to be carried out. This represents a very significant development in the realm of molecular beam technology as prior to this no other $O(^1D_2)$ beam source has been reported in the literature.

$O(^1D_2)$ production was experimentally confirmed in our universal crossed molecular beam apparatus by observing the production of OH from the reaction

$$O(^1D_2) + H_2 \longrightarrow OH + H \qquad \Delta H = -43.5 \text{ kcal/mole} \qquad (9)$$
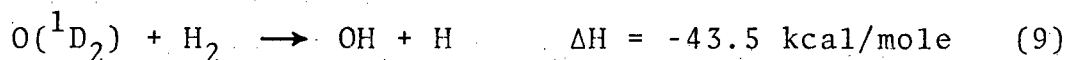
For this study a supersonic hydrogen beam (peak velocity = 2.66×10^5 cm/sec, Mach number = 21) was collided at 90° with an oxygen seeded in helium beam (peak atomic oxygen velocity = 2.38×10^5 cm/sec, Mach number = 9) at a relative collision energy of 2.7 kcal/mole. The oxygen beam was produced by discharging a 200 torr, 5% O_2-He gas mixture

with 200 watts of RF power. Under these experimental
conditions the OH could not have been produced by the
ground state reaction

$$O(^3P_J) + H_2 \longrightarrow OH + H \qquad \Delta H = 1.9 \text{ kcal/mole} \qquad (10)$$

due to the large 8.9 kcal/mole activation energy[33] which
is associated with this process. Further support of the
Reaction (9) process comes from the angular and velocity
distributions of the OH reaction product. The OH LAB angular
distribution shown in Fig. 15 extends as far as the OH(v=0)
Center-of-Mass velocity circle permits based upon a reaction
exoergicity of 43.5 kcal/mole, while the OH velocity distri-
butions obtained with cross correlation time-of-flight
techniques[34,35] fall off with velocities indicative of
this exoergicity. These experimental distributions also
indicate that the concentration of $O(^1S_0)$ atoms in the
terminal beam must be extremely low as no OH product was
observed at the high energies characteristic of the process

$$O(^1S_0) + H_2 \longrightarrow OH + H \qquad \Delta H = -94.7 \text{ kcal/mole} \qquad (11)$$

When 10% O_2-He gas mixtures were discharged rather than

5% O_2-He mixtures a 30% decrease in OH signal was observed relative to the 3000 counts/sec counting rate of the more dilute mixture. This indicates that the number of collisions occurring between $O(^1D_2)$ atoms and other oxygen species should be minimized during the expansion if extensive quenching of the $O(^1D_2)$ is to be avoided. When dilute oxygen-argon gas mixtures were tested no OH product was detected, indicating that, within the accuracy of the determination, oxygen seeded in argon beams contain no $O(^1D_2)$. This is fortunate as it enables $O(^3P_J)$ reactions to be studied in an environment free of $O(^1D_2)$ contamination when argon is used as the beam carrier gas.

The presence of $O(^1D_2)$ in beams having helium as the carrier gas can be attributed to the extremely small quenching rate constant of the process

$$O(^1D_2) + He(^1S_0) \longrightarrow O(^3P_J) + He(^1S_0)$$

$$\Delta H = -45.4 \text{ kcal/mole} \tag{12}$$
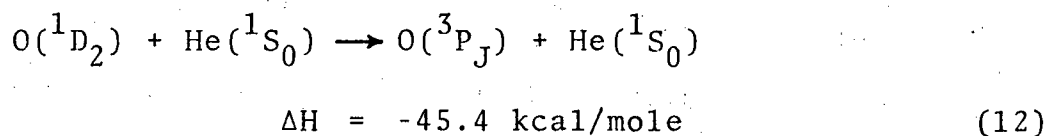
which has been experimentally found to be: $k^Q_{O-He} < 10^{-16}$ cm^3 molecule^{-1} sec^{-1}.[36] This value can be compared to the "gas kinetic" rate constant in order to crudely estimate the number of collisions needed for quenching to occur:

$k_{O-He}^{GK} \approx 8 \times 10^{-10}$ cm^3 molecule^{-1} sec^{-1}. This gas kinetic rate constant was approximated by $k^{GK} = (\pi r_m^2)(\frac{8kT}{\pi\mu})^{1/2}$, where r_m is the experimentally determined Lennard-Jones (12,6) parameter for $O(^3P_J)$-He collisions,[37] T is the plasma temperature, taken as 1000K, and μ is the reduced mass of the collision partners. The above indicates that, on the average, about 10^6 $O(^1D_2)$-He collisions must occur before quenching takes place. Since only about 10^2 collisions occur during the expansion[38] it is not sur-prising that some $O(^1D_2)$ atoms are present in the terminal beam. In fact, most $O(^1D_2)$ quenching probably occurs during collisions between $O(^1D_2$ and other oxygen species which are present in the beam. In contrast to this, the experimentally determined rate constant for $O(^1D_2)$ quenching by Ar, $k_{O-Ar}^Q = 3 \times 10^{-13}$ cm^3 molecule^{-1} sec^{-1},[36] is only about three orders of magnitude smaller than the O-Ar "gas kinetic" rate constant, $k_{O-Ar}^{GK} \approx 6 \times 10^{-10}$ cm^3 molecule^{-1} sec^{-1}, which was calculated assuming a plasma temperature of 1500K and using the r_m value for $O(^3P_J)$-Ar given by Reference 37. The $O(^1D_2)$-Ar collisions therefore deactivate a significant fraction of the $O(^1D_2)$ atoms during expansion, with the remaining $O(^1D_2)$ atoms being deactivated by collision with the other atomic and molecular oxygen species which are present in the beam ($k_{O-O_2}^Q = 3.7 \times 10^{-11}$ cm^3 molecule^{-1} sec^{-1}).[36] An analysis of the collision dynamics

for Reaction (9) is currently being prepared for publication, and will be presented elsewhere in the literature.

The pressure and power dependence of $O(^1D_2)$ production has been examined for a 5% O_2-He gas mixture in our crossed beam apparatus. This was accomplished by monitoring, at the peak of the broad product angular distribution, the OH signal intensity coming from Reaction (9) as a function of beam source pressure and RF power level. Since the oxygen and hydrogen beam velocities are nearly equal the OH count rate is indicative of the $O(^1D_2)$ particle flux. (Whereas if the hydrogen beam were much faster than the oxygen beam the OH count rate would be indicative of the $O(^1D_2)$ number density at the collision center.) The curved shape of the intensity versus pressure data shown in Fig. 16a indicates that some $O(^1D_2)$ quenching does occur at higher pressures, but not to the extent which would require operating the sources at pressures below 250 torr. The intensity versus RF power curves shown in Fig. 16b clearly indicate that higher source powers (and hence plasma temperatures) significantly increase the flux of $O(^1D_2)$ emanating from the nozzle. In the near future gas mixtures composed of less than 5 percent oxygen will be characterized in order to determine the optimum oxygen-helium mixture for maximizing $O(^1D_2)$ production.

DISCUSSION

The high pressure, supersonic, radio frequency discharge beam source which has been described in the preceeding sections of this paper offers several improvements in the important operating characteristics of beam translational energy, beam intensity, velocity distribution width, and beam composition when compared to either thermal or low pressure discharge effusive sources. For example, the atomic oxygen translational energies which have been accessed in our laboratory span the range from 0.1-0.5 eV, with future extension of this range up to 0.7 eV being possible for operation with dilute oxygen-helium mixtures. These energies are considerably higher than those accessible with effusive sources constructed from either thoria (ThO_2)[39] or iridium.[40] Also, the atomic oxygen intensity produced by an effusive thermal oven, operating with Knudsen number = 1, would be ca. 4×10^{16} atoms sr^{-1} sec^{-1}.[41] This intensity was calculated using an O_2 pressure of 1 torr, a calculated equilibrium constant of K_p = 1.2×10^{-2} torr for the process $O_2 \rightleftharpoons 2O$ at 2500K, and assuming that the source orifice was 2 mm high. The fluxes available from low pressure discharge sources are comparable to this, with atomic oxygen fluxes of ca. 3×10^{16} atoms sr^{-1} sec^{-1} being realized for operation under effusive flow conditions (with 10% molecular

dissociation, a temperature of 350K,[42] Knudsen number = 1, and a slit height of 2 mm). The above atomic oxygen intensities are much lower than the measured intensities produced by our seeded nozzle source: ca. 5×10^{17} atoms $sr^{-1} sec^{-1}$ for oxygen-argon mixtures and $\geq 5 \times 10^{18}$ atoms $sr^{-1} sec^{-1}$ for oxygen-helium mixtures. Also note that the Maxwellian velocity distributions typical of effusive sources are quite often too broad for carrying out well defined collision experiments, necessitating the use of mechanical velocity selectors which further reduce their intensity by at least an order of magnitude. It is there-fore evident that the nozzle source described here is capable of producing atomic oxygen fluxes which are at least 1-3 orders of magnitude higher than those possible with conventional effusive sources, with the actual inten-sity gain depending upon the peak velocity and velocity widths which are used for this comparison. The high atomic oxygen fluxes produced by this source should permit extremely well defined collision experiments to be carried out in which the supersonic beam source would be coupled with either a high resolution mechanical velocity selector or with a magnetic sublevel quantum state selector in order to further define the atomic beam.

The ability of this source to generate seeded beams having high molecular dissociation at pressures up to several hundred torr total pressure is undoubtedly due to plasma localization at the nozzle tip and to the highly efficient power coupling which has been achieved between the RF tank circuit and the plasma. The use of radio frequency rather than microwave power simplified the above as radio frequency generated plasmas can be easily drawn out of the region enclosed by the coupling coil, while microwave generated plasmas tend to strongly localize in the region surrounded by the coupling cavity. The facile frequency variability and impedance matching of the RF circuitry described earlier also simplifies operation at high pressures. The water cooled nozzle, which ensures extremely stable and reproducible day to day operation of the source, would have to be replaced with a more cumbersome and less efficient oil-cooled design if microwave radiation were used. The ability of this source to generate terminal beams containing $O(^1D_2)$ atoms is at this time unique, and would not have been possible if the discharge were removed from the region immediately behind the orifice.

The atomic oxygen is probably generated in the discharge by a variety of kinetic processes. Thompson[43] has shown, for low pressure discharges, that dissociation can

be directly induced by electron-O_2 collisions via the Schumann-Runge continuum $O_2(^3\Sigma_g^-) \rightarrow [O_2(^3\Sigma_u^-)] \rightarrow O(^3P_J) + O(^1D_2)$ for collision energies > 7.1 eV. Metastable argon collisions could also lend to dissociation via this process.[11] Metastable helium atoms, due to their high energies, have the ability to Penning ionize molecular oxygen. Ionization in this manner, followed by dissociative recombination between O_2^+ and an electron has been proposed as the primary source of atomic oxygen in oxygen-helium RF discharges.[8]

The generation of other atomic and electronically excited species should also be possible with this source. In our laboratory we have briefly tested dilute hydrogen-helium mixtures (125 torr total pressure, 145 watts) and have observed atomic hydrogen production. The generation of a supersonic molecular beam containing $O_2(^1\Delta_g)$ *without* the simultaneous presence of atomic oxygen in the terminal beam should be possible. This could be accomplished by pulling the discharge back, away from the nozzle tip, and by introducing a small amount of mercury into the gas mixture. The resulting mercuric oxide coating located after the discharge zone would effectively remove the atomic species present in the gas.[44] The feasibility of generating atomic nitrogen beams with a high temperature

version of this source is currently being explored in our laboratory.

ACKNOWLEDGEMENT

REFERENCES

1. J. T. Herron and R. E. Huie, J. Phys. Chem. Ref. Data, 2, 467 (1973).

2. S. J. Arnold and H. Rojeska, Appl. Opt. 12, 169 (1973).

3. R. J. Madix and A. A. Susu, Surface Sci. 20, 377 (1970).

4. W. D. McGrath and J. J. McGarvey, Planet. Space. Sci. 15, 427 (1967).

5. R. J. Cvetanović, Advan. Photochem. 1, 115 (1963).

6. J. B. Anderson, R. P. Andres, and J. B. Fenn, in Adv. Chem. Phys., Vol. 10, J. Ross, Ed. (John Wiley and Sons, New York, 1966), p.275.

7. N. Abauf, J. B. Anderson, R. P. Andres, J. B. Fenn, and D. G. H. Marsden, Science 155, 997 (1967).

8. D. R. Miller and D. F. Patch, Rev. Sci. Instrum. 40, 1566 (1969).

9. P. A. Gorry, C. V. Nowikow, and R. Grice, Chem. Phys. Lett. 49, 116 (1977).

10. AD-998 alumina: Coors Porcelain Company, Golden, Colorado, USA.

11. H. S. Johnston, Gas Phase Reaction Kinetics of Neutral Oxygen Species, Chemical Kinetics Information Center, Nat. Stand. Ref. Data Sys., Nat. Bur. Stand. 20, (U.S. Government Printing Office, Washington, D.C., 1968), p.4.

12. H. G. Wagner and J. Wolfrum, Angew. Chem. Internat. Edit. <u>10</u>, 604 (1971).

13. F. K. McTaggart, <u>Plasma Chemistry in Electrical Discharges</u> (Elsevier, Amsterdam, 1967), p.38.

14. The Radio Amateur's Handbook, 46th ed., D. DeMaw, Ed. (ARRL, Newington, 1969), p.44.

15. The Radio Amateur's Handbook, 46th ed., D. DeMaw, Ed. (ARRL, Newington, 1969), p.49.

16. Radio Engineering Handbook, 5th ed., K. Henny, Ed. (McGraw-Hill, New York, 1959), Chap.18, p.23.

17. Model MN-2000: R. L. Drake Company, Miamisburg, Ohio, U.S.A.

18. Paddlewheel flowswitch: Perkin-Elmer Ultek, Inc., Palo Alto, California, U.S.A.

19. Carborundum hot pressed boron nitride: Carborundum Co., Refractories and Electronics Division, Latrobe, Pennsylvania, U.S.A.

20. Y. T. Lee, J. D. McDonald, P. R. LeBreton, and D. R. Herschbach, Rev. Sci. Instrum. <u>40</u>, 1402 (1969).

21. M. S. Child, <u>Molecular Collision Theory</u> (Academic, New York, 1974), p.3.

22. W. L. Fite and R. T. Brackman, Phys. Rev. <u>113</u>, 815 (1959).

23. D. Rapp, P. Englander-Golden, and D. D. Broglia, J. Chem. Phys. <u>42</u>, 4081 (1965).

24. J. B. Anderson and J. B. Fenn, Phys. Fluids, $\underline{8}$, 780 (1965).

25. J. J. Valentini, Ph.D. dissertation, University of California, Berkeley, California, 1976.

26. D. H. Levy, L. Wharton, and R. E. Smalley, in Chemical and Biochemical Applications of Lasers, C. B. Moore, Ed. (Academic, New York, 1977), Vol. 2, p.1.

27. D. R. Miller and R. P. Andres, in Sixth Rarefied Gas Dynamics, L. Trilling and H. Wachman, Eds. (Academic, New York, 1969), Vol. 2, p.1385.

28. D. R. Miller and R. P. Andres, J. Chem. Phys. $\underline{46}$, 3418 (1967).

29. J. G. Skofronik, Rev. Sci. Instrum. $\underline{38}$, 1628 (1967).

30. G. Scoles and F. Torello, "Production of Molecular Beams from Free Expanding Jets, Part 1", Report of the Gruppodi Strutture Della Materia del C.N.R., August 1967.

31. Scientific Foundations of Vacuum Techniques, S. Dushman and J. M. Lafferty, Eds. (John Wiley and Sons, New York, 1962), p.324.

32. J. B. Anderson, R. P. Andres, and J. B. Fenn, in Molecular Beams, J. Ross, Ed. (John Wiley and Sons, New York, 1966) p.312.

33. D. L. Baulch, D. D. Drysdale, D. G. Horne, and A. C. Lloyd, Evaluated Kinetic Data for High Temperature Reactions (Butterworth, London, 1972), Vol. 1a, p.49.

34. V. L. Hirschy and J. P. Aldridge, Rev. Sci. Instrum. 42, 381 (1971).

35. K. Sköld, Nucl. Instrum. Meth. 63, 114 (1968).

36. K. Schofield, J. Photochem. 9, 55 (1978).

37. V. Aquilanti, G. Liuti, F. Pirani, F. Vecchiocattivi, and G. G. Volpi, J. Chem. Phys. 65, 4751 (1976).

38. J. J. Valentini, private communication.

39. W. Espe, Materials of High Vacuum Technology Vol. 12 - Silicates, (Pergamon, Oxford, 1968) p.564.

40. P. L. Moore, P. N. Clough, and J. Geddes, Chem. Phys. Lett. 17, 608 (1972).

41. H. Pauly and J. P. Toennies, in Methods of Experimental Physics, B. Bederson and W. L. Fite, Eds. (Academic, New York, 1968), Vol. 7A, p.232.

42. D. St. A. G. Radlein, J. C. Whitehead, and R. Grice, Mol. Phys. 29, 1813 (1975).

43. J. B. Thompson, Proc. Roy. Soc. A. 262, 503 (1961).

44. A. M. Winer and K. D. Bayes, J. Phys. Chem. 70, 302 (1966).

FIGURE CAPTIONS

Fig. 1.   Sectioned view of the plasma beam source mounted
           in a differentially pumped chamber. A-Lucite
           insulating flange. B-Nozzle coolant return.
           C-Quartz nozzle gas inlet. D-Cajon ultra-torr
           fittings. E-Nozzle coolant inlet. F-RF power
           input from RG-213/U coaxial cable. G-Variable
           air capacitor. H-Coupling coil coolant outlet.
           I-Coupling coil coolant inlet. J-Ceramic feed-
           through for RF return and coil coolant. K-Ceramic
           feedthrough for RF input and coil coolant.
           L-Poly-Flo tubing sections. M-Stainless steel
           source chamber. N-Plates for 5000 V/cm ion
           deflecting field. O-1200 1/sec diffusion pump,
           differential region. P-4200 or 8000 1/sec
           diffusion pump, source region. Q-Epoxy resin
           mechanical support. R-Electrical ground wire.
           Not shown: Wire mesh RF shielding which covers
           the air capacitor/RF feedthrough assembly.

Fig. 2.   Sectioned view of the internal source components.
           A-Variable ground tap. B-Swagelock reducer.
           C-Water-cooled quartz nozzle. D-Coupling coil.
           E-Quartz support rod for water inlet/outlet
           assembly. F-Swagelock union joining copper and

Polyflow tubing. G-Cajon VCO fitting. H-Kovar-
pyrex section. I-Graded seal, pyrex to vycor.
J-Aluminum support block to electrical ground.
K-Boron nitride skimmer, 0.88 mm. L-4X enlarge-
ment of nozzle tip; arrows indicate low conduc-
tivity water flow direction.

Fig. 3. Impedance matching circuitry.

Fig. 4. Block diagram of the plasma generating electronics.
The double solid lines indicate the equipment used
for high power operation, while the double dashed
lines indicate the bypassing necessary for pre-
liminary tune-up of the source.

Fig. 5. a) Newton diagrams for O-He and O_2-He elastic
scattering. b) Differential elastic scattering
cross sections for O-He and O_2-He. The wide
angle falloff of the O-He curve conclusively
demonstrates atomic oxygen production.

Fig. 6. Pressure dependence of O_2 dissociation:
O 5% O_2-Ar, 165 watts; ● 5% O_2-Ar, 130 watts;
△ 10% O_2-Ar, 195 watts; □ 10% O_2-Ar, 140 watts;
■ 5% O_2-He, 130 watts; ▲ 10% O_2-He, 130 watts;
◊ 10% O_2-He, 165 watts; — — — performance data
for the source described in Reference 8.

Fig. 7.   R.F. power dependence of O_2 dissociation.

⬤   5% O_2-Ar, 250 torr;   ⬤   10% O_2-Ar, 250 torr.

☐   10% O_2-He, 175 torr.

Fig. 8.   Pressure dependence of atomic beam velocity.

⬤   5% O_2-He, 130 watts;   ⬤   10% O_2-He, 165 watts,

△   10% O_2-He, 130 watts;   ☐   10% O_2-Ar, 195 watts;

◼   5% O_2-Ar, 165 watts;   ▲   5% O_2-Ar, 130 watts;

◇   10% O_2-Ar, 140 watts.

Fig. 9.   R.F. power dependence of atomic beam velocity.

⬤   5% O_2-He, 200 torr;   ⬤   10% O_2-He, 175 torr;

◼   5% O_2-Ar, 250 torr;   ☐   10% O_2-Ar, 250 torr.

Fig. 10.   Atomic oxygen velocity distribution for a seeded
           beam having a FWHM of 19%. The solid line is
           the deconvoluted best fit to the experimental
           data which yields a beam Mach number of 9.2.

Fig. 11.   Pressure dependence of atomic beam Mach number.

⬤   5% O_2-He, 130 watts;   ⬤   10% O_2-He, 130 watts;

◇   10% O_2-Ar, 195 watts;   △   5% O_2-Ar, 130 watts;

☐   5% O_2-Ar, 165 watts;   ◼   10% O_2-He, 165 watts.

Fig. 12.   R.F. power dependence of atomic beam Mach number.

⬤   10% O_2-He, 175 torr;   △   10% O_2-Ar, 250 torr;

⬤   5% O_2-Ar, 250 torr.

Fig. 13. R.F. power dependence of plasma temperature.

○ 5% O_2-Ar, 250 torr;   ●   10% O_2-Ar, 250 torr;

□ 10% O_2-He, 175 torr.

Fig. 14. a) Atomic oxygen number density as a function of

pressure for argon containing mixtures.

○ 10% O_2-Ar, 195 watts;   ●   5% O_2-Ar, 165 watts.

b) Atomic oxygen number density as a function of

pressure for helium containing mixtures.

○ 10% O_2-He, 165 watts;   ●   5% O_2-He, 130 watts.

These curves have all been corrected for slight

m/e = 16 contributions arising from dissociative

ionization of mass 32 in the electron bombardment

ionizer.

Fig. 15. Laboratory angular distribution of OH from the

reaction $O(^1D_2)$ + H_2 → OH + H at a relative

collision energy of 2.7 kcal/mole. The solid

line is a calculated fit to the experimental

data which employed a symmetrical center-of-mass

product distribution for the OH product. The

excellent fit between the calculated and experi-

mental data, taken in conjunction with with wide

angle falloff (~40°) of the distribution,

demonstrates the presence of $O(^1D_2)$ atomic oxygen

in the terminal beam.

Fig. 16.   a) Relative $O(^1D_2)$ intensity as a function of
gas pressure for a 5% O_2-He, 200 watt discharge.
b) Relative $O(^1D_2)$ intensity as a function of
R.F. power level for a 5% O_2-He gas mixture.
● 150 torr total pressure; O 100 torr total
pressure.   These curves indicates that the
$O(^1D_2)$ intensity can optimized by simultaneously
operating the source at high power and pressure
settings.
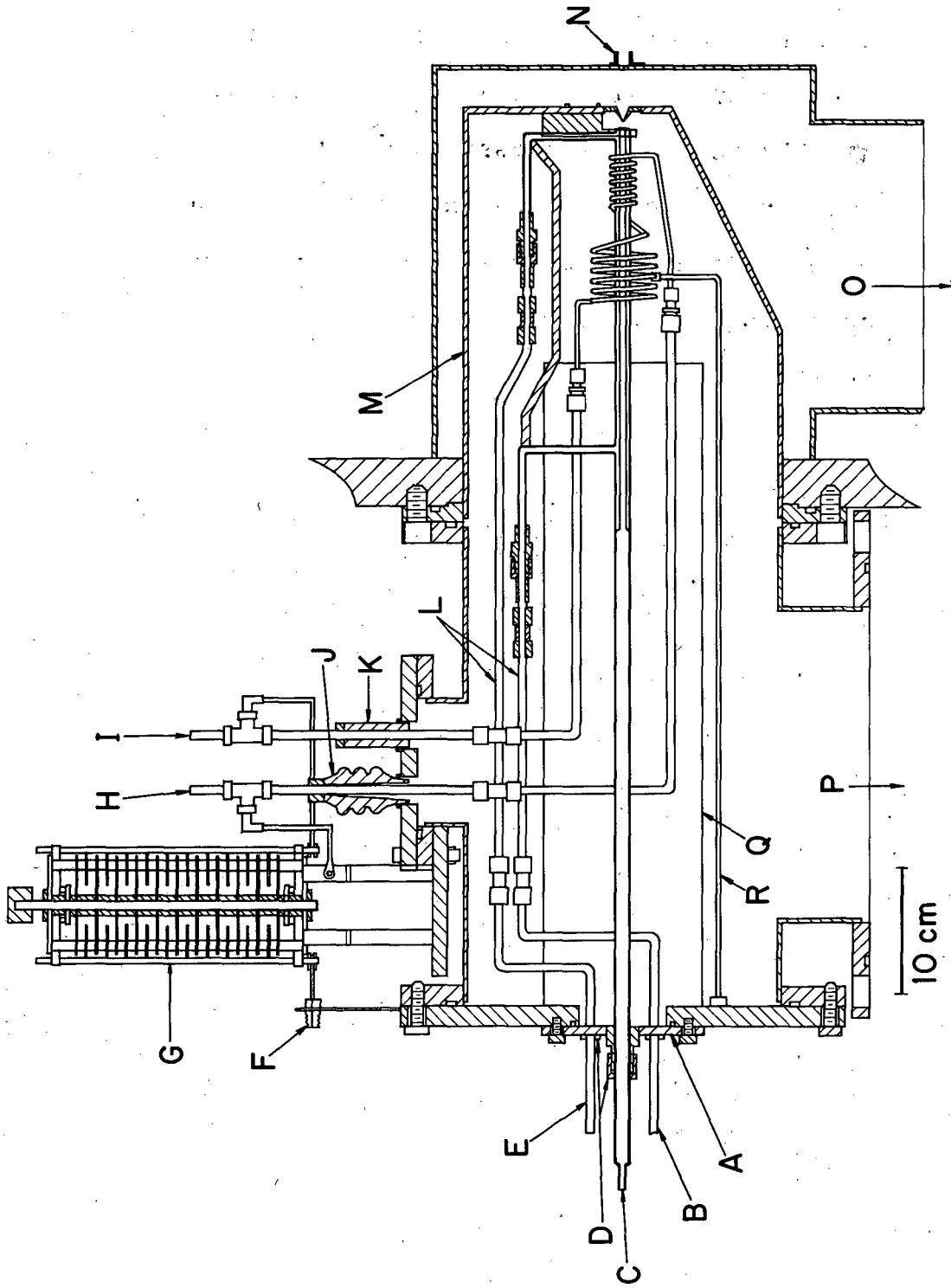
Fig. 1

XBL 782 - 2881.

XBL782-2882

Fig. 2

-68-
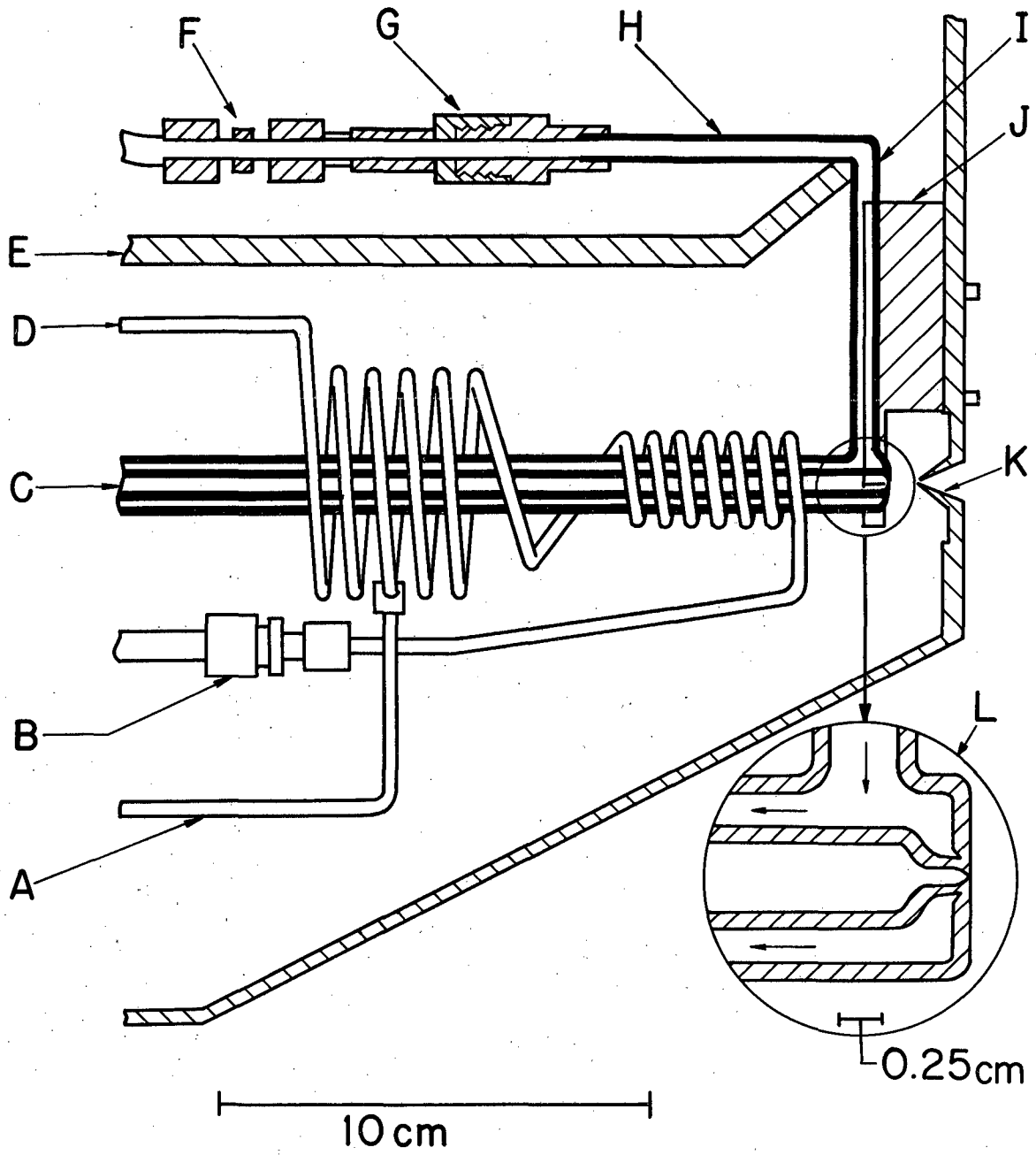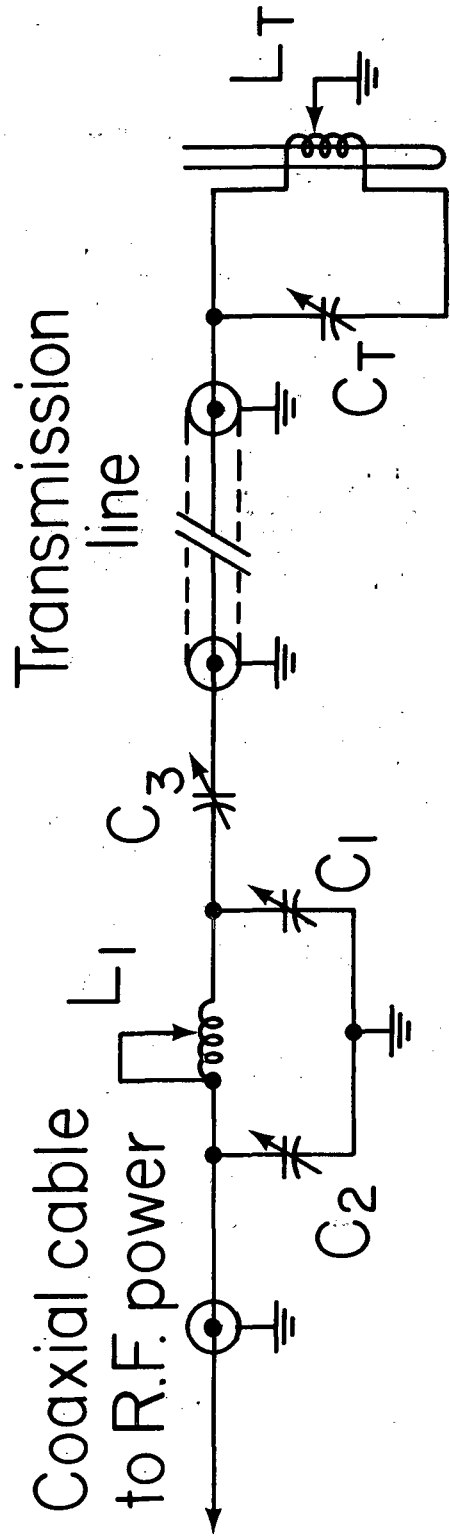
Fig. 3
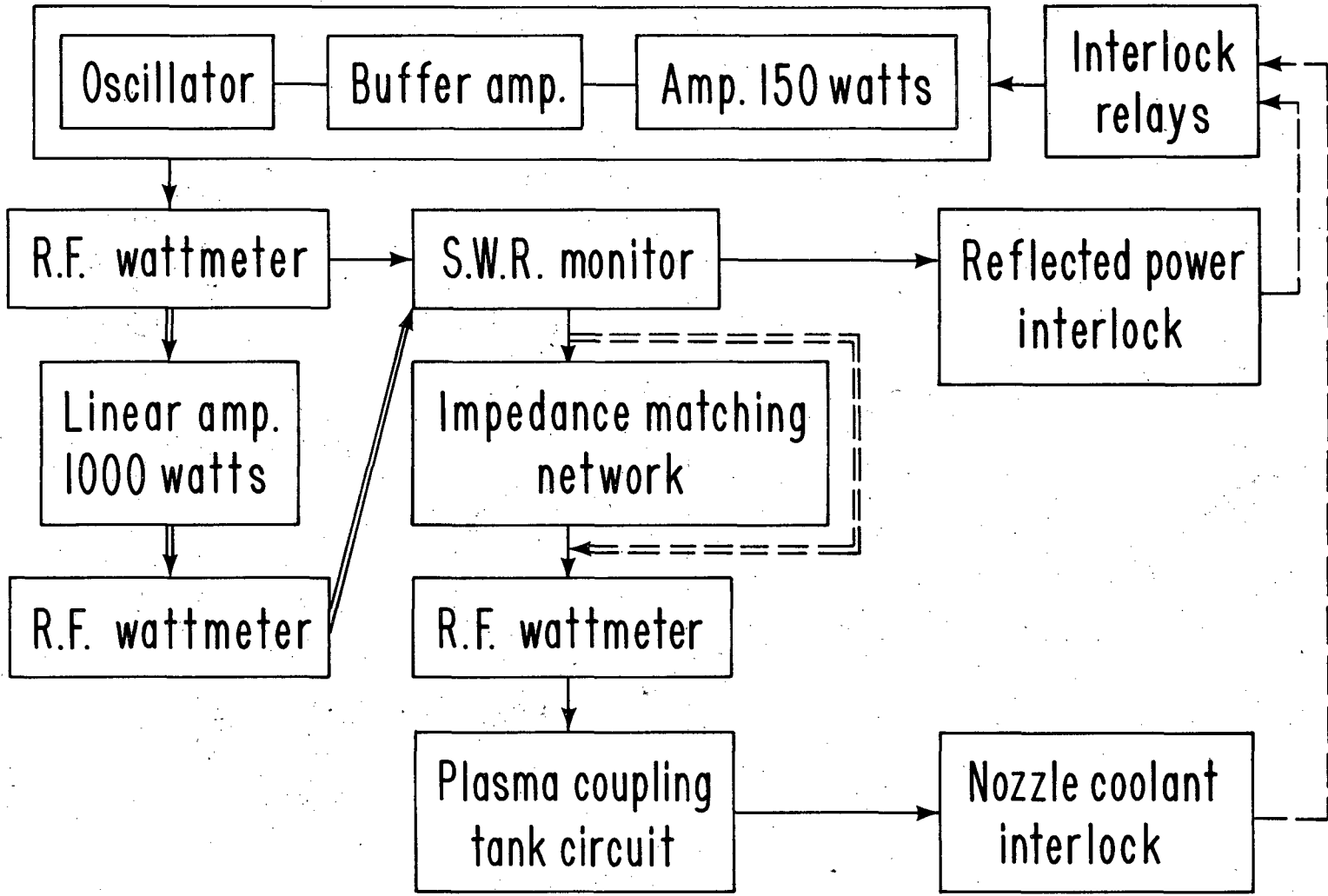
XBL 797-2255

Fig. 4
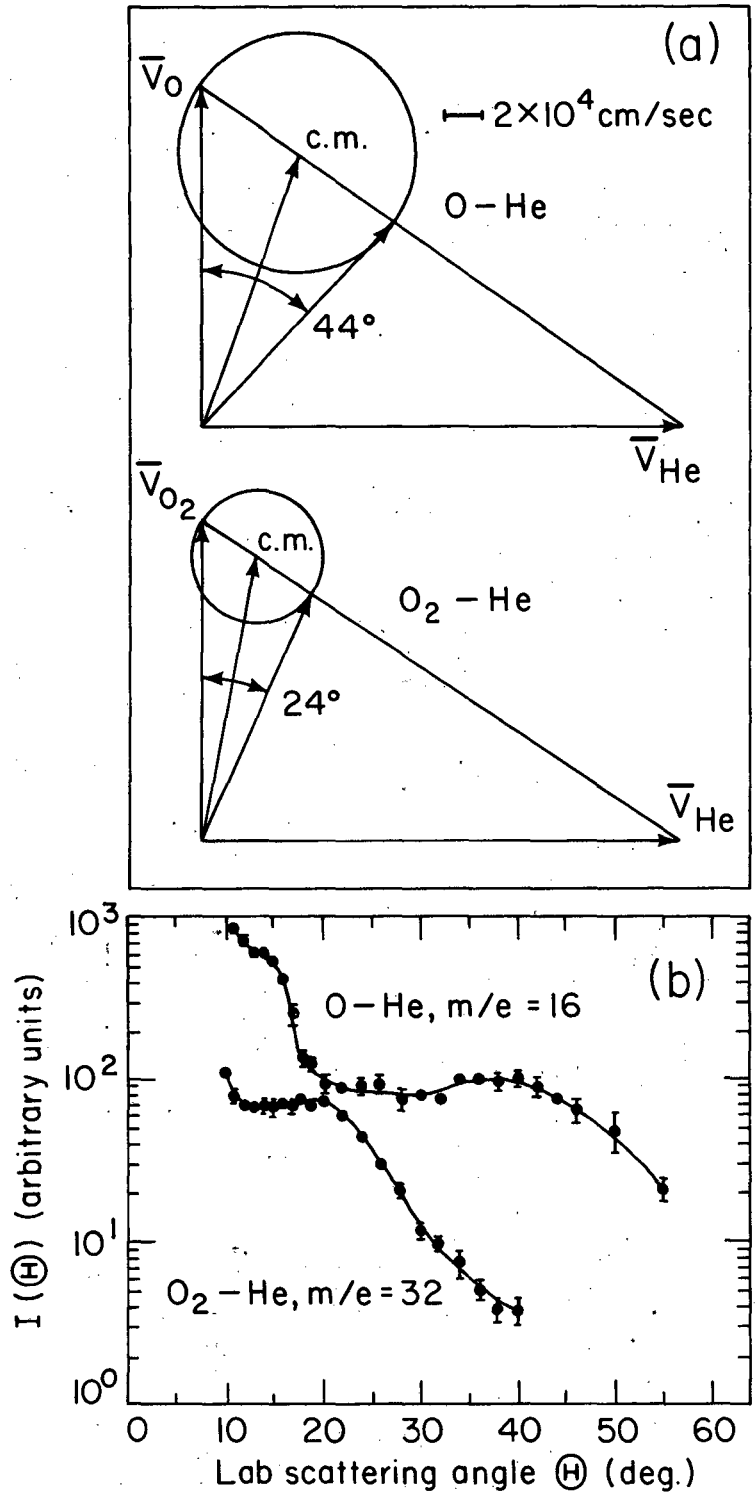
XBL 797-2257

Fig. 5
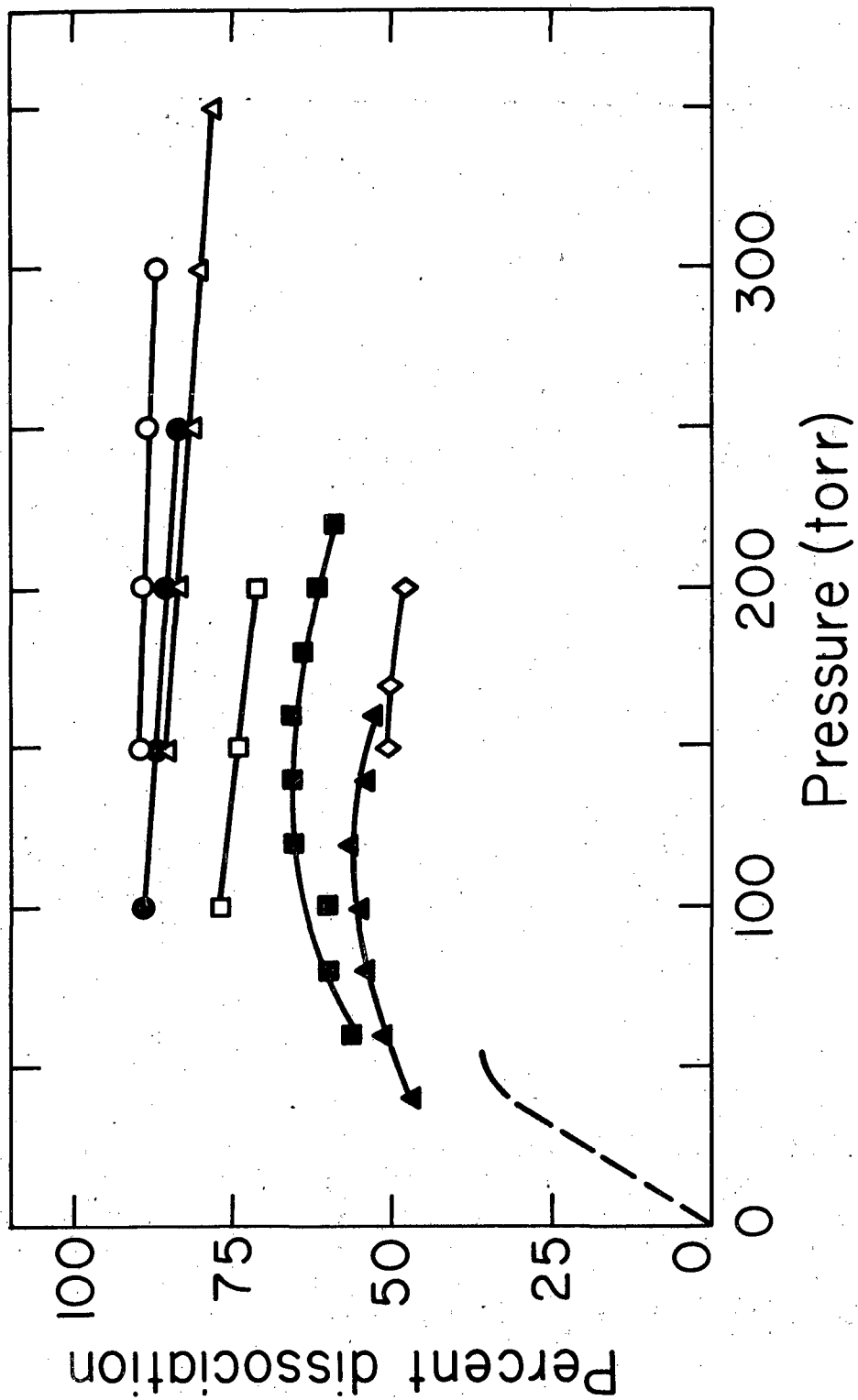
Fig. 6

XBL 797-2259
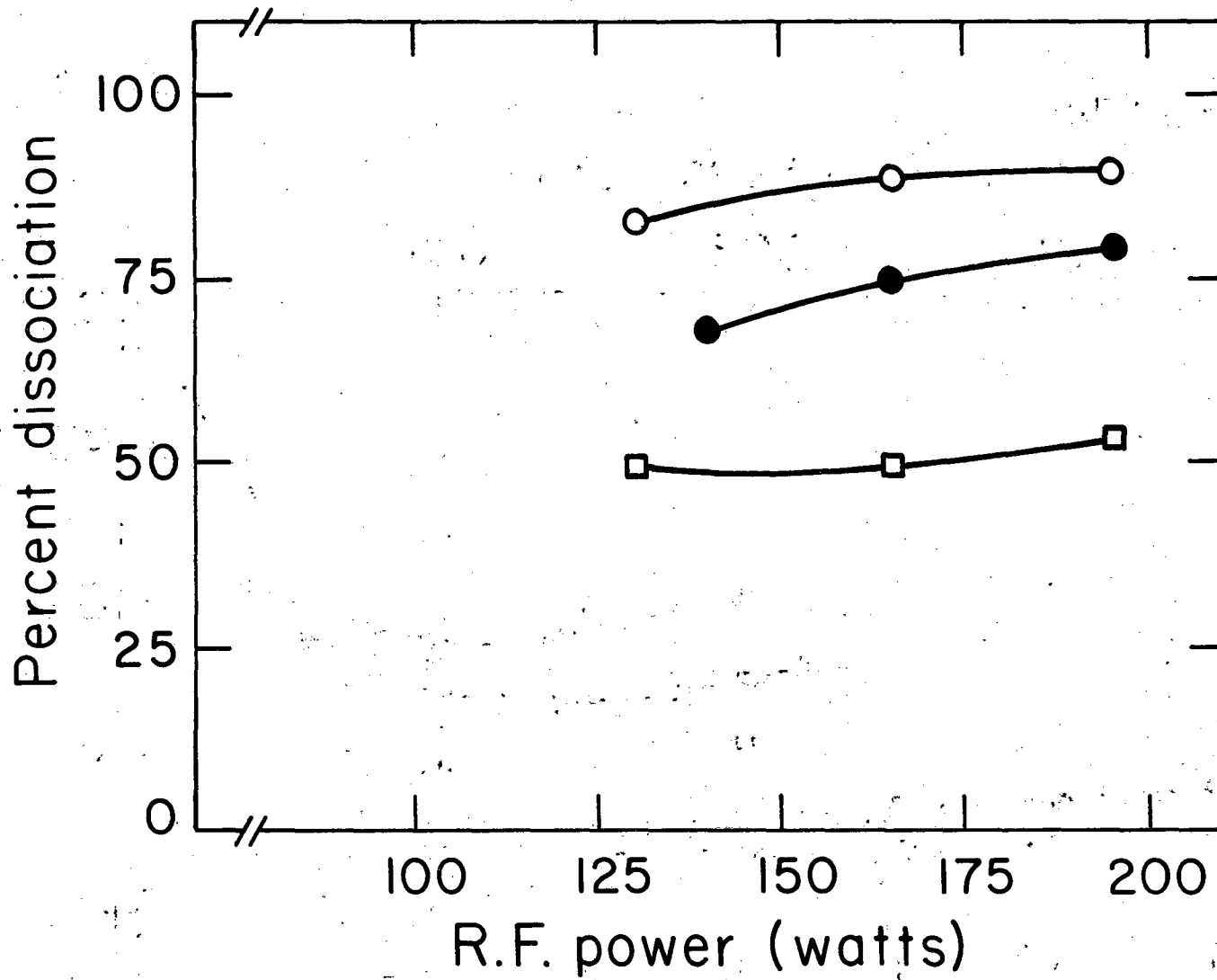
Fig. 7   XBL 797-2264
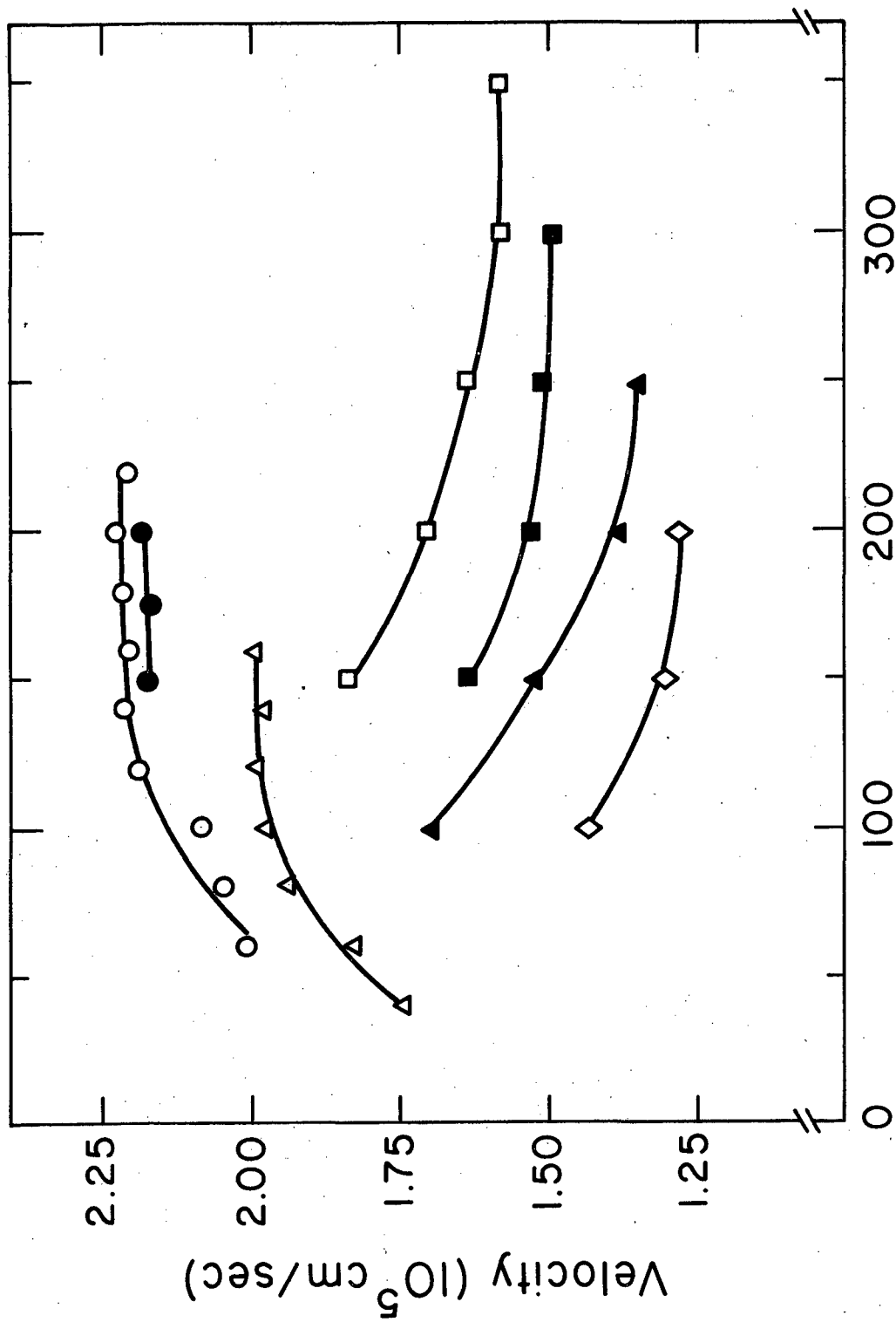
Fig. 8

XBL 797-2263

XBL 797-2262

Fig. 9

Fig. 10

XBL 797-2265

Pressure (torr)

Mach number
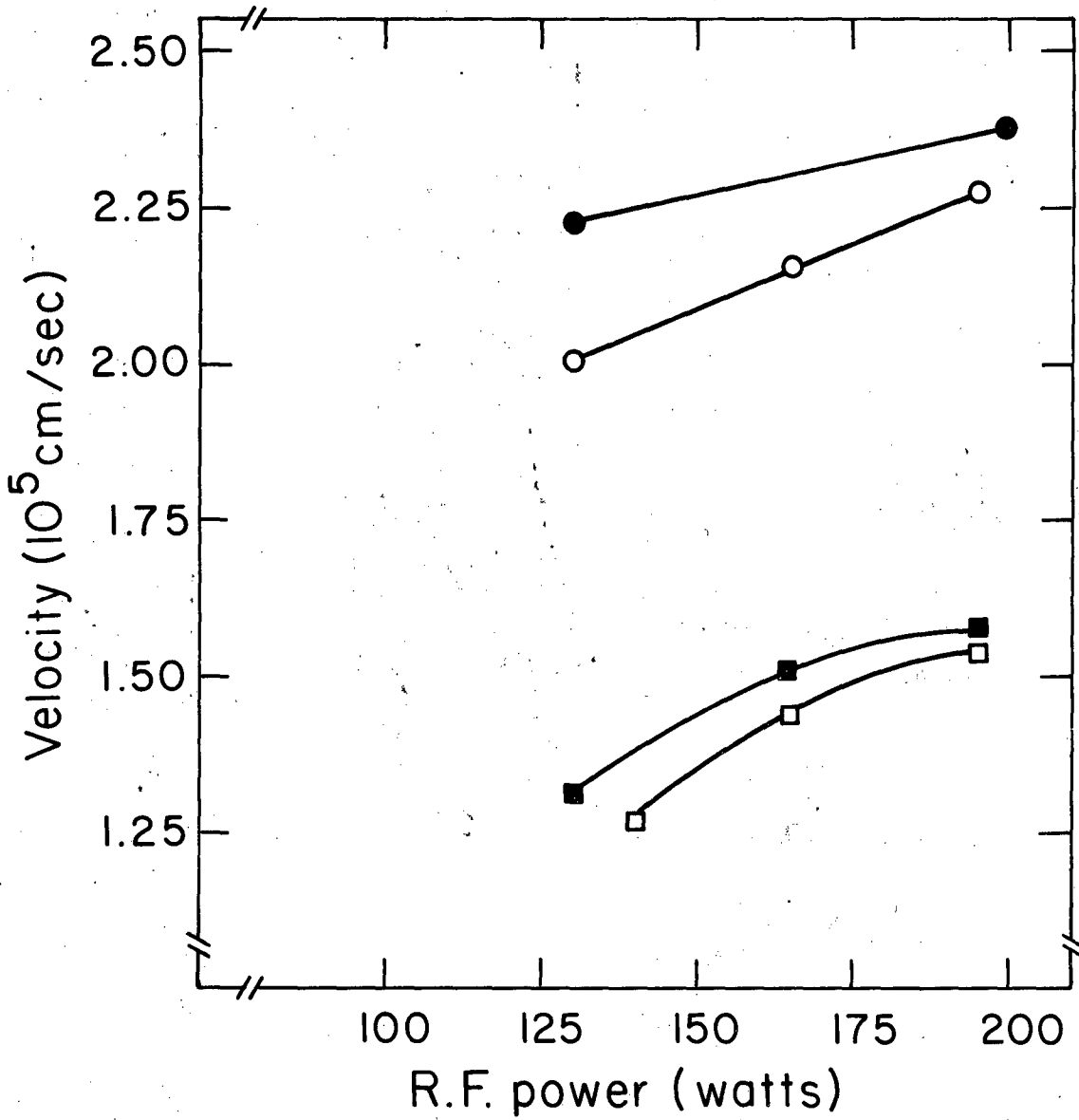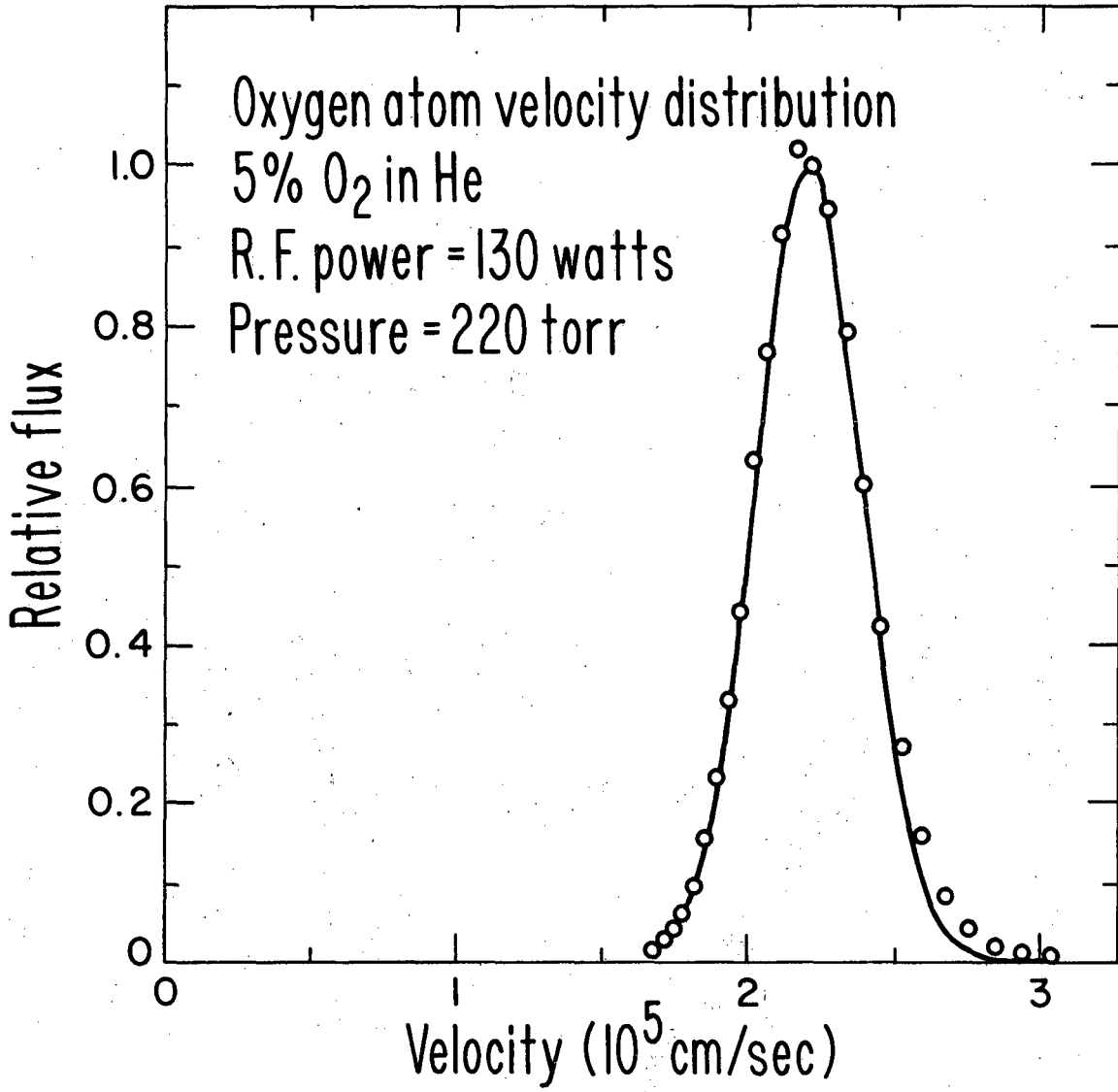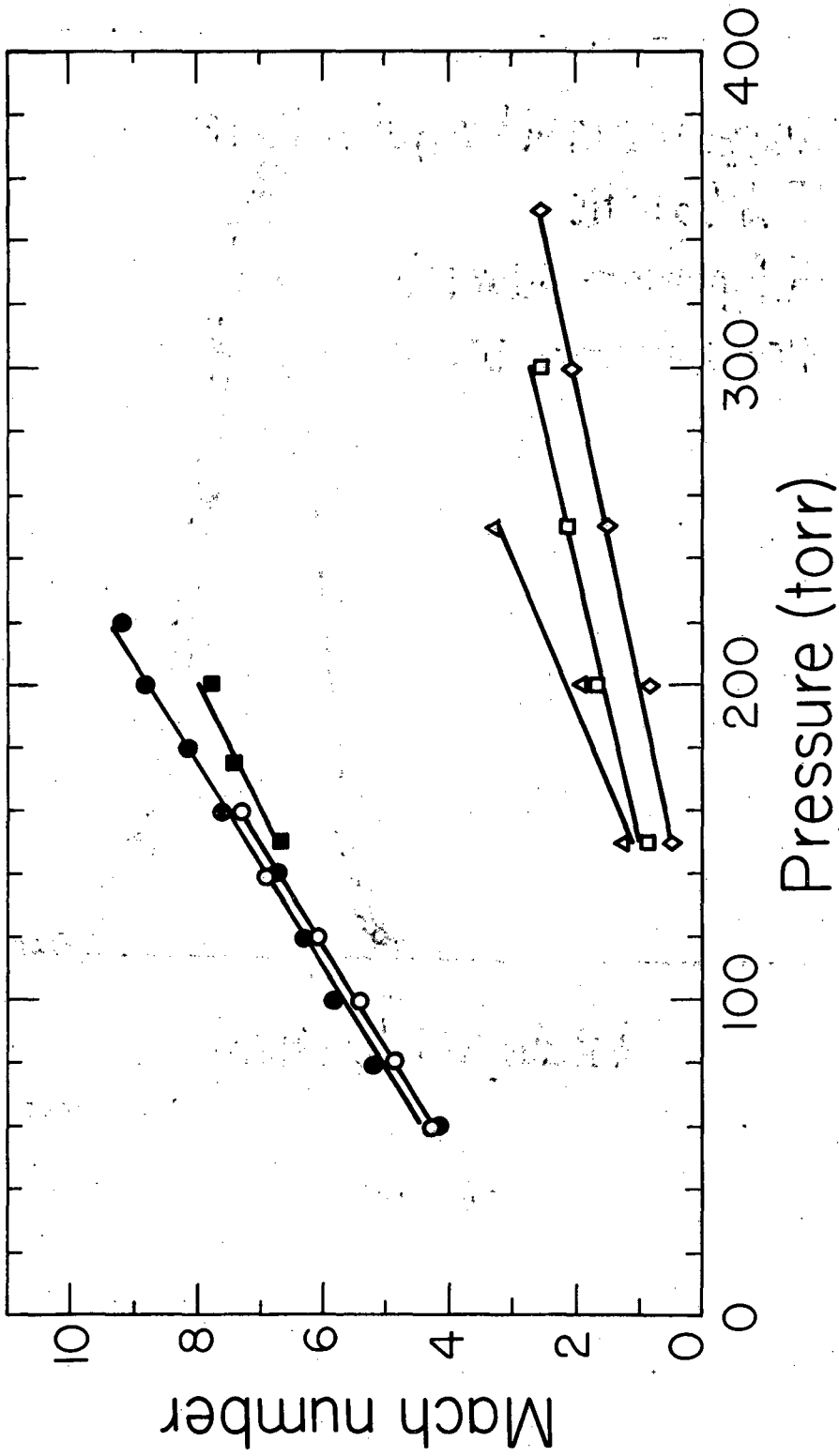
Fig. 11
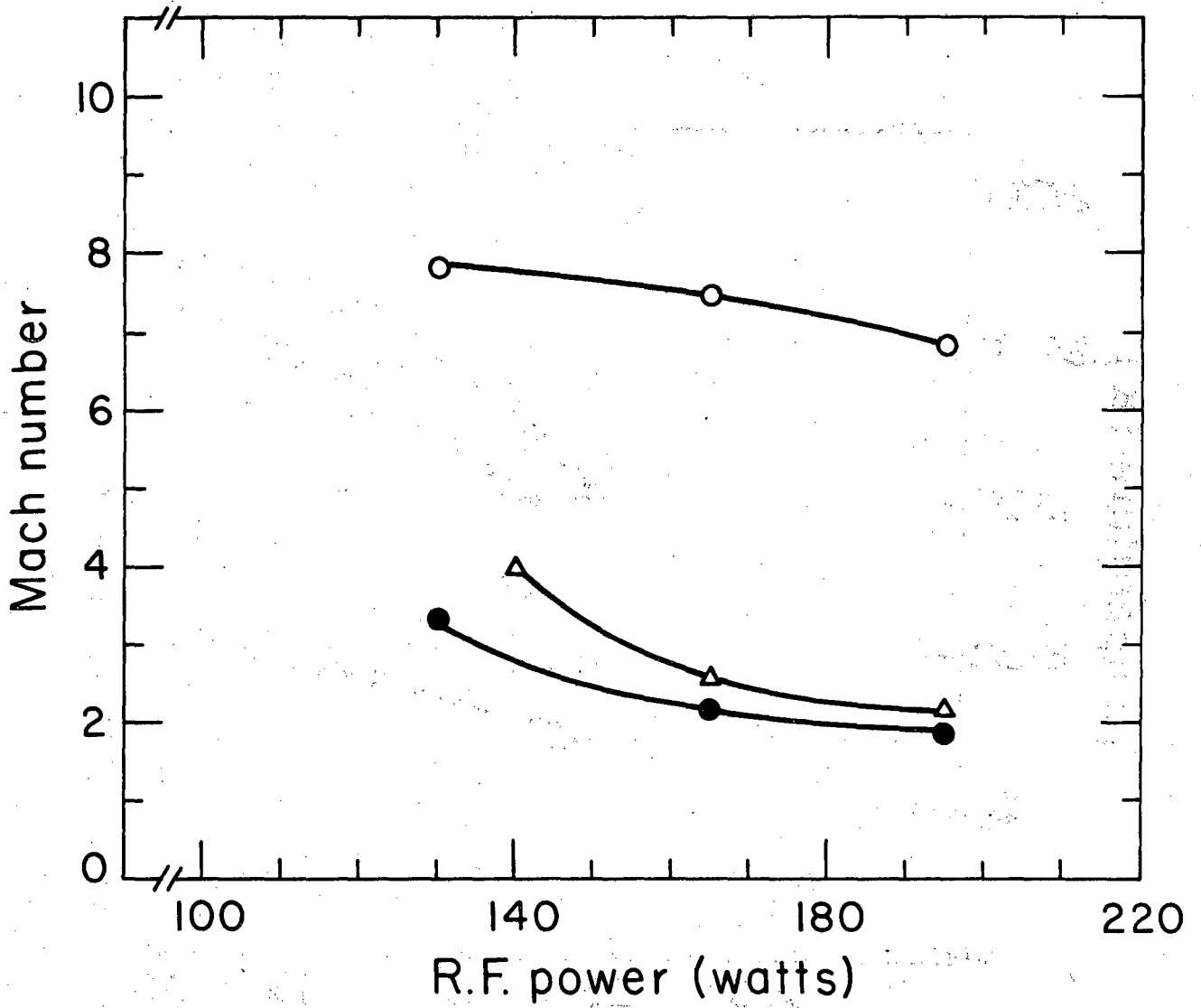
XBL 797-2258

XBL 797-2261

Fig. 12
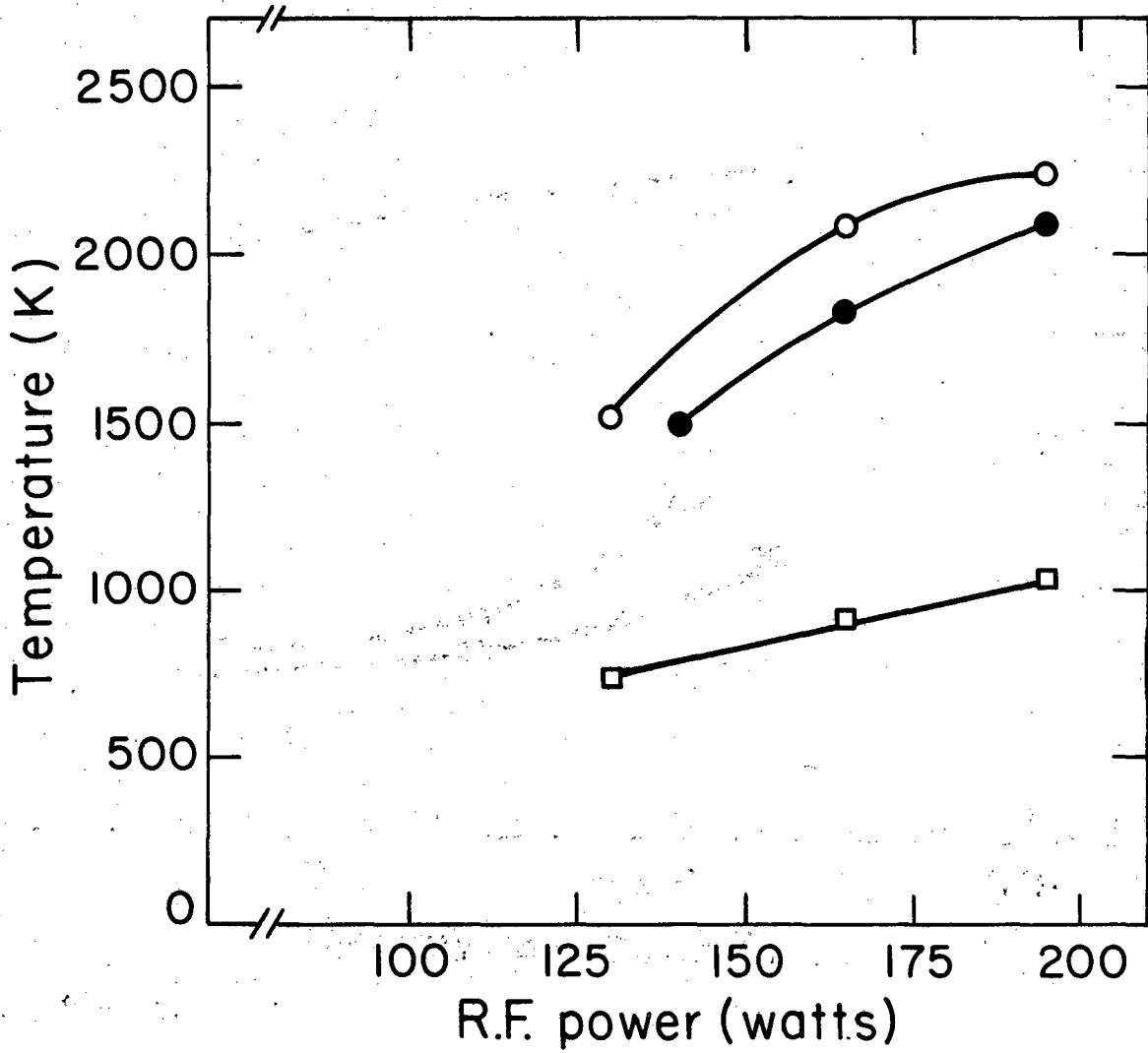
XBL 797-2260

Fig. 13
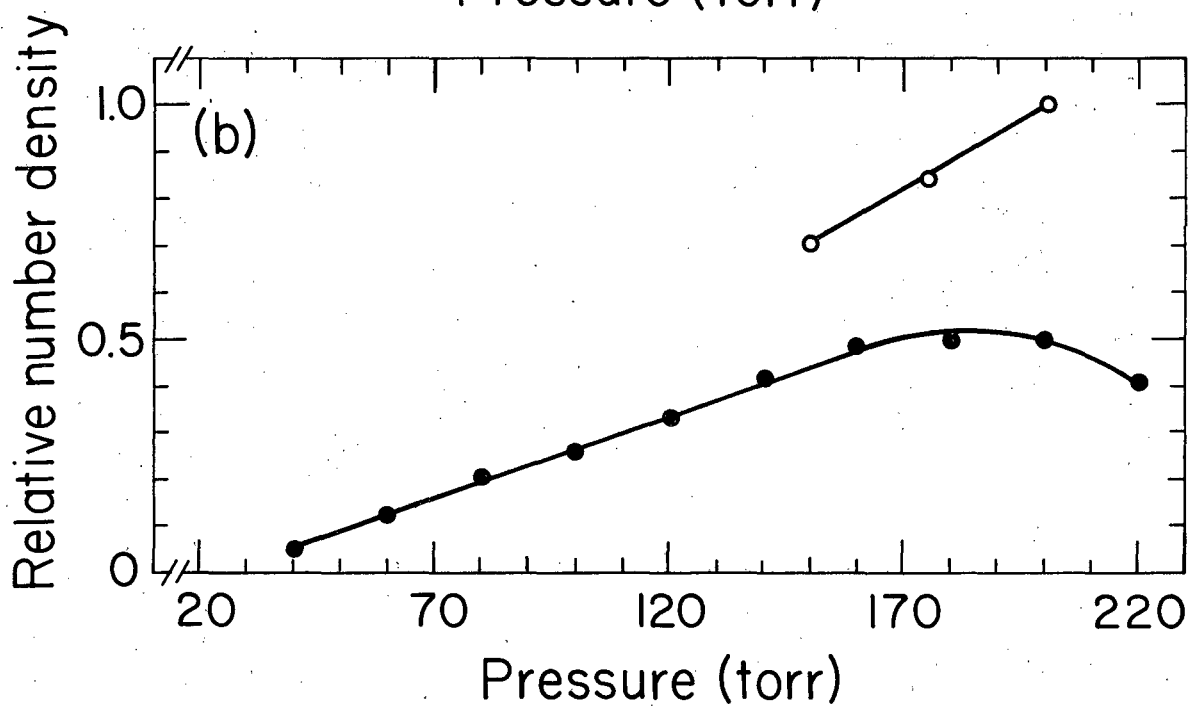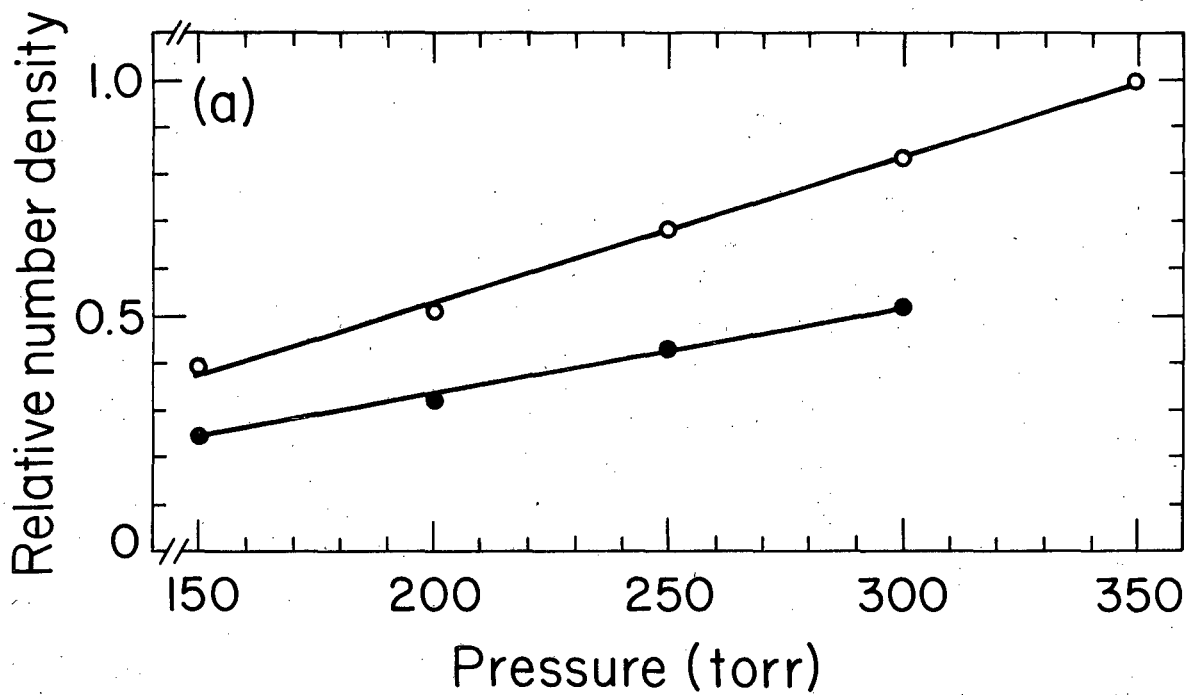
XBL 797-2254

Fig. 14
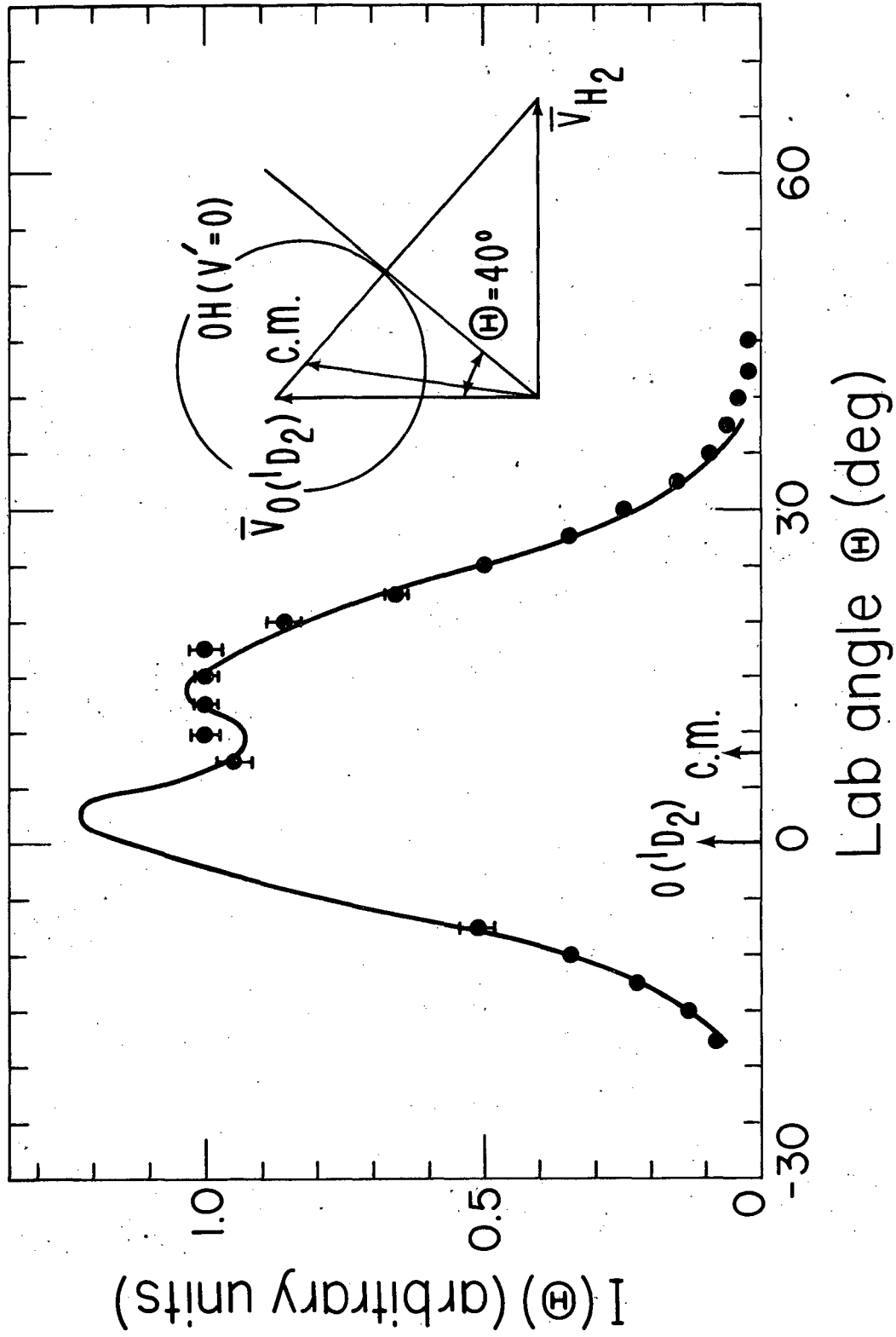
Fig. 15
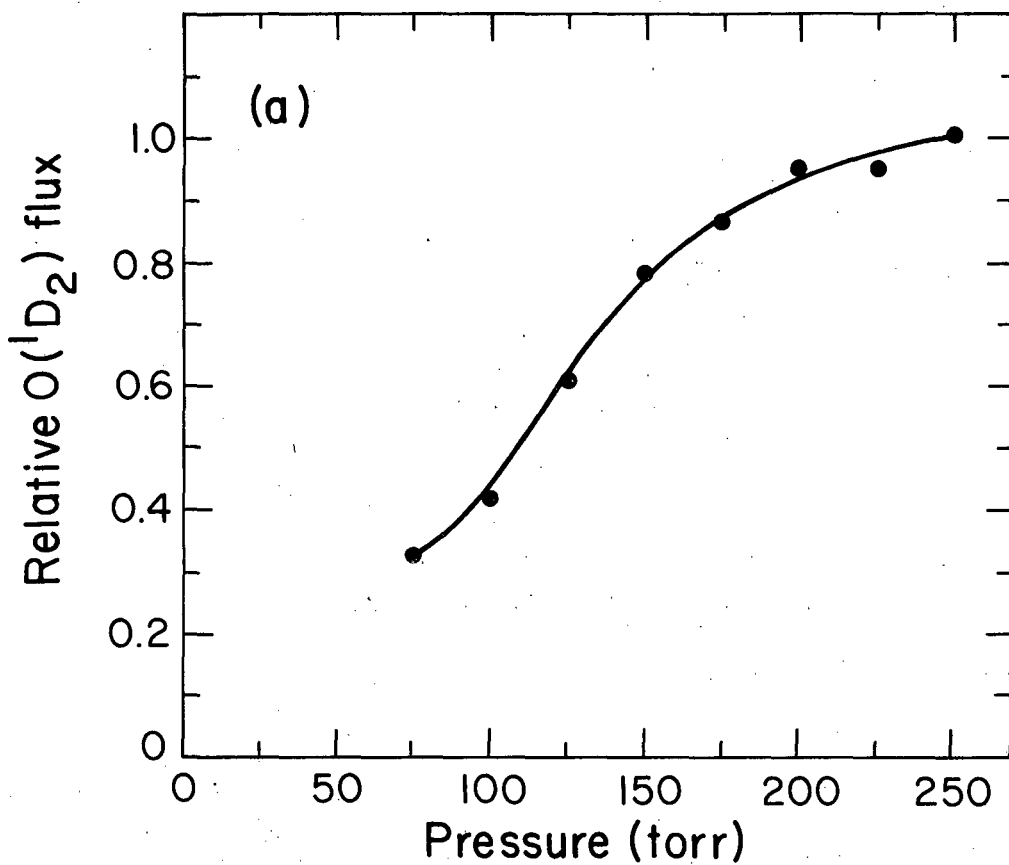
XBL 797-2253

XBL 797-2256

Fig. 16